Coordination Assemblies of Acetylenic Dithioether Ligands on Silver(I) Salts: Crystal Structure, Antibacterial and Cytotoxicity Activities

Quentin Gaudillat, Jan-Lukas Kirchhoff, Isabelle Jourdain, Vincent Humblot, Agathe Figarol, Michael Knorr, Carsten Strohmann, Lydie Viau

Coordination Assemblies of Acetylenic Dithioether Ligands on Silver(I) Salts: Crystal Structures, Antibacterial and Cytotoxicity Activities

Quentin Gaudillat,[1] Jan-Lukas Kirchhoff,[2] Isabelle Jourdain,[1] Vincent Humblot,[3] Agathe Figarol,[3] Michael Knorr,[1] Carsten Strohmann,[2] Lydie Viau[1*]*

[1] Université de Franche-Comté, UMR CNRS 6213, Institut UTINAM, 16 Route de Gray, F-25000 Besançon, France lydie.viau@univ-fcomte.fr; isabelle.jourdain@univ-fcomte.fr

[2] Anorganische Chemie, Technische Universität Dortmund, Otto-Hahn-Straße 6, 44227 Dortmund, Germany

[3] Université de Franche-Comté, UMR CNRS 6174, Institut FEMTO-ST, 15B avenue des Montboucons, 25030 Besançon, France

Abstract

Coordination polymers (CPs) and Metal Organic Frameworks (MOFs) constitute a new class of antibacterial materials. Their interest stems from their wide range of topology, dimensionality, and secondary building unit that can be tuned by an appropriate choice of metal ions and ligands. Especially, silver-based ones feature good antibacterial properties. In this study, six novel coordination polymers (CPs) were obtained by the coordination of three acetylenic dithioether $RSCH_2C{\equiv}CCH_2SR$ (R = phenyl (L_{Ph}), cyclohexyl (L_{Cy}), tert-butyl (L_{tBu}) ligands on several silver salts (silver tosylate, silver triflate and silver trifluoroacetate). The crystallographic characterization evidenced the formation of a molecular macrocycle or CPs with different dimensionalities, ranging from 1D to 2D. In most cases, they are composed of four-coordinated silver atoms in a tetrahedral environment. Their antibacterial activity was investigated against both Gram-positive (*Staphylococcus aureus*) and Gram-negative (*Escherichia coli*) bacteria. All CPs present good antibacterial properties against the tested bacteria with minimal inhibitory concentration (MIC) values going from 5 to 40 μg Ag per mL. Interestingly, we found that these values could not be correlated to their architecture or morphology nor to the amount of silver released. The cytotoxicity of these compounds was also evaluated on normal human dermal fibroblasts (NHDF) and three out of these CPs were found biocompatible.

Introduction

Penicillin, a heterocyclic compound featuring a β-lactam scaffold, was the first antibacterial molecule discovered by Alexander Fleming in 1928.[1] However, the first signs of bacterial resistance were observed by Abraham and Chain with the inactivation of penicillin by *E. coli*.[2] According to the World Health Organization, the antimicrobial resistance (AMR) is one of the top global public health threats and is responsible for millions of deaths. To circumvent the antibacterial resistance, up to the sixties, the number of new antibiotics has increased exponentially. However, after this golden age, only few novel organic structures featuring a noteworthy biological activity were discovered. Whereas academic institutions have increased their efforts in this field, pharmaceutical companies are facing decreasing profits and have therefore neglected research activities to develop novel antibiotics.[3] On the other side, metallic silver has been known since antiquity for its antimicrobial properties.[4, 5] The

discovery of new potent antibiotics has put aside research activities on silver compounds during the second half of the 20th century. The renewed interest in silver-based compounds, especially nanoparticles has arose to the fact that silver is claimed not to induce any antimicrobial resistance.[6] Indeed, contrary to organic antibiotics that target a specific site, silver has several modes of action. Silver salts, like silver nitrate, exhibit string antimicrobial activities but their high aqueous solubility led to elevated silver concentrations causing tissues damage.[7] To circumvent this problem, the solubility of the salt should be controlled. As example, silver sulfadiazine that contains a huge organic (4-amino-*N*-2-pyrimidinylbenzenesulfonamidato) anion has a lower solubility than an inorganic salt and therefore ionic silver is thus only slowly released upon its ionization in body fluids.[8] Other forms of silver that have been used for antibacterial applications are for example nanoparticles (NPs) with various shape and form.[9-13] These nanosilvers can be found in various consumer products like refrigerators, clothes, cosmetics, or medical instruments like catheters. For food applications, silver particles were mixed with different non-degradable (polyethylene,[14, 15] polyvinyl chloride) and biodegradable polymers (cellulose, chitosan).[16, 17] Dental biomaterials were also prepared by incorporation of AgNPs in composite resins, acrylic resins and implants.[18] Nowadays, one of the key point in the development of antibacterial materials is to manage the content and rate of silver release while staying in a therapeutic window.

Silver(I) presents a versatile coordination geometry and coordination numbers ranging from two to six. The most numerous complexes are those that are two-, three- and four-coordinated while the five- and six-coordinated ones are scarcer.[19] This rich coordination flexibility has led to the development of various silver complexes, coordination polymers (CPs), and Metal-Organic Frameworks (MOFs) especially for biomedical applications.[20, 21] Depending on the experimental conditions, the nature of the silver salts and the ligands, numerous silver-based CPs and MOFs with different topologies and dimensionalities have been described. Especially silver-based CPs and MOFs containing *N*- and *O*-donor ligands have been developed.[22-32] Most of them present good antibacterial activities attributed to the fact that these ligands exert weak binding affinity toward silver atoms leading to a relatively high release of silver. If a high silver release led to high antibacterial efficiency, as stipulated above, this amount should be controlled in order to fit within the therapeutic window.

According to the Pearson's HSAB theory,[33] the combination soft donor ligands-soft Lewis acid should lead to a higher chemical stability compared to the one obtained with hard donor ligands. Recently, we have communicated the first examples of two antibacterial silver-based

CPs constructed from the assembly of soft-donor ligands with the soft-Lewis acid Ag(I).[34] These 2D CPs were obtained by coordination of rigid acetylenic dithioether $RSCH_2C{\equiv}CCH_2SR$ ligands with silver nitrate. In these two CPs, the coordination sphere around the silver atoms was the same, the main structural differences relying on the coordination mode of the ligands (2- or 4-electron donors). When suspended in aqueous media, these CPs slowly release silver atoms that are responsible for their antibacterial properties. Also, we found a good relationship between their antibacterial performance, the amount of silver deliverance and their structural stability. However, as many other studies related to that field, we did not measure their cytotoxicity effect. We thus decided to put forward our study and prepared a series of CPs obtained by coordination of three different acetylenic dithioether ligands (L_{Ph} = 1,4-bis(phenylthio)-2-butyne, L_{Cy} = 1,4-bis(cyclohexylthio)-2-butyne, and $L_{t\mathrm{Bu}}$ = 1,4-bis(tert-butylthio)-2-butyne) on different silver salts namely silver tosylate (AgOTs), silver triflate (AgOTf) and silver trifluoroacetate ($AgCF_3CO_2$). We chose to modulate the bulkiness and nucleophilicity of the -SR group as this may impact the strength of the -SR→Ag bond. Also, we probed different anions with various coordination mode to tune the architecture of the materials. The modulation of all these parameters was expected to lead to CPs with structural diversity and accordingly, different antibacterial properties.

Indeed, we succeed to prepare six new CPs with dimensionalities ranging from 0D to 2D. NON 0D is not a CP The architectures of these CPs were determined by single-X-Ray diffraction studies and their characterization was completed by IR spectroscopy, elemental analyses, scanning electron microscopy, powder X-ray diffraction studies as well as thermal analyses. We then studied their antibacterial performances by measurement of their minimal inhibitory concentration (MIC) against Gram-negative *Escherichia coli* and Gram-positive *Staphylococcus aureus* bacteria and evaluated their bactericidal activity by time-killing assays. Finally, the *in vitro* biocompatibility of these CPs was attested on human fibroblasts.

Results and discussion

Synthesis and crystallographic description

The molecular structure of the dithioether acetylenic ligands used in this study with their acronym is given in Figure 1. These ligands were prepared by nucleophilic substitution of 1,4-dichlorobut-2-yne with the corresponding thiolate.[34, 35] They were then coordinated to different silver salts and the following results are given as a function of the silver salt type.

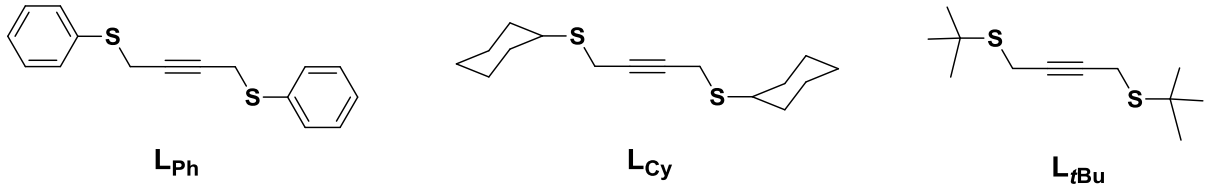

Figure 1. Structures of the acetylenic ligands used in this study.

Coordination to silver tosylate

Structure of $[Ag(L_{Ph})_{1.5}(OTs)]_n$ CP1

CP1 was prepared by reaction of AgOTs with L_{Ph} using a 1:1 molar ratio in acetonitrile (scheme 1).

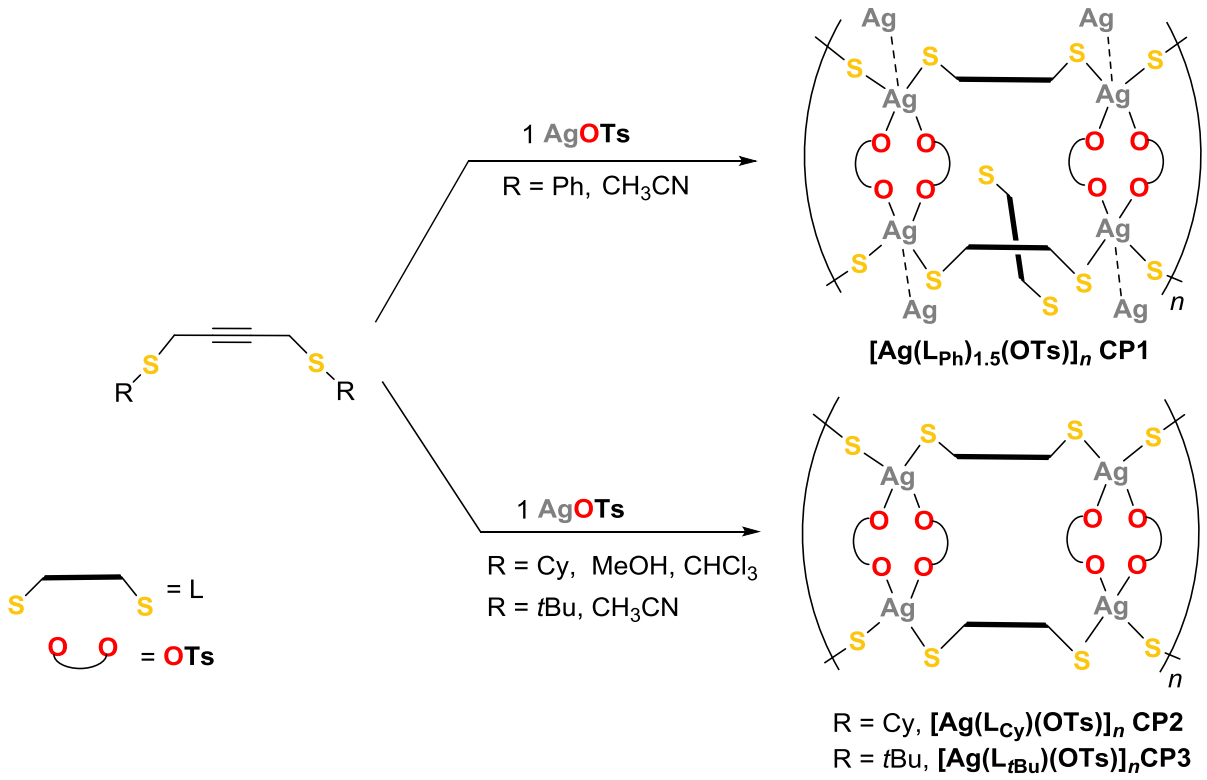

Scheme 1. Reaction of silver tosylate (AgOTs) with L_{Ph}, L_{Cy} and L_{tBu} forming **CP1**, **CP2**, and **CP3**.

Single-crystal X-ray diffraction (SCXRD) analysis revealed that compound **CP1** crystallizes in the triclinic $P\bar{1}$ space group, and the crystal parameters are listed in Table S1. As illustrated in Figure S1, the asymmetric unit consists of one Ag(I) ion, one L_{Ph} ligand, one tosylate anion and one-half of a non-coordinated L_{Ph} ligand. The elemental analysis of the isolated product confirmed an $Ag(OTs)(L_{Ph})_{1.5}$ composition. Repeated experiments always led to the formation of this product containing co-crystallized ligand L_{Ph} in a 1:0.5 ratio. In **CP1,** each silver atom is four-coordinated in an AgO2S2 distorted tetrahedral environment (if neglecting the Ag–Ag interactions) by two oxygen atoms from two different tosylate anions (d(Ag–O) = 2.4030(15) and 2.5311(15) Å) and by two S atoms from distinct ligands (d(Ag–S) = 2.5024(6) and 2.5253(6) Å) with S/O-Ag-S/O angles spanning the range 87.03(4)-139.535(18)°. The τ_4 geometry index[36] was calculated according to: $\tau_4 = [360 - (\alpha + \beta)]/141$ (where α and β are the largest angles around the metal center) and found to be equal to 0.69.

Two tosylate anions chelate two silver atoms via two out of their three oxygens atoms in a μ_2-(κ^1O^1:κ^1O^2) coordination mode leading to the formation of a dimer. Each L_{Ph} ligand is in a *cis* configuration and bridges two silver atoms of these dimers resulting in the formation of a 1D ribbon extending to the *b* direction. The repeating unit of these double chains consists of a 22-membered $Ag_4(L_{Ph})_2O_4S_2$ metallamacrocycle. Furthermore, the distance between the Ag···Ag atoms ($d_{Ag\cdots Ag}$ = 3.2242(4) Å), which is shorter than twice the van der Waals radii of the Ag^+ ion (3.44 Å),[37] indicates the presence of unsupported argentophilic interactions in the framework.[38] These argentophilic interactions cause the expansion of **CP1** to the 2D-dimension and the formation of a second 16-membered $Ag_4(L_{Ph})_2$ metallamacrocycle (Figure S2). Uncoordinated L_{Ph} molecules are also present in the interlamellar regions (Figure S3) and are anchored to the ribbon via C-H···π interactions between the triple bond of the coordinated ligand and H29 of the phenyl ring on an uncoordinated ligand (Figure S4). Geometrical parameters for the C29-H29···C≡C interactions are listed in Table S4. Contrary to the coordinated L_{Ph} ligands, the uncoordinated ones are in a *transoïd* configuration. There are also several other C–H···A (A = O, S) and C-H···π interactions that stabilize the structure (Table S5 and Figure S4). The coordination mode of **CP1** is reminiscent of that encountered in 1D CP $[\{Ag\{\mu\text{-}PhS(CH_2)_3SPh\}(OTs)]_n$ (CSD ref code TAXXIA) reported by Brisse *et al.*[39] Comparison of the main distances with this CP can be found in Table S6. The average Ag–S distance is slightly shorter in **CP1** (2.5138(6) *vs.* 2.537(1) Å) but the mean Ag–O distance is

longer (2.4670 (15) *vs.* 2.410(5) Å). The major difference between the structures arises from the absence of any Ag···Ag interactions in [{Ag{μ-PhS$(CH_2)_3$SPh}(OTs)]$_n$. In **CP1**, all phenyl rings of the ligands are parallelly aligned along the *b* axis without showing any π-π interactions. However, such arrangement allows for the formation of Ag···Ag interactions.

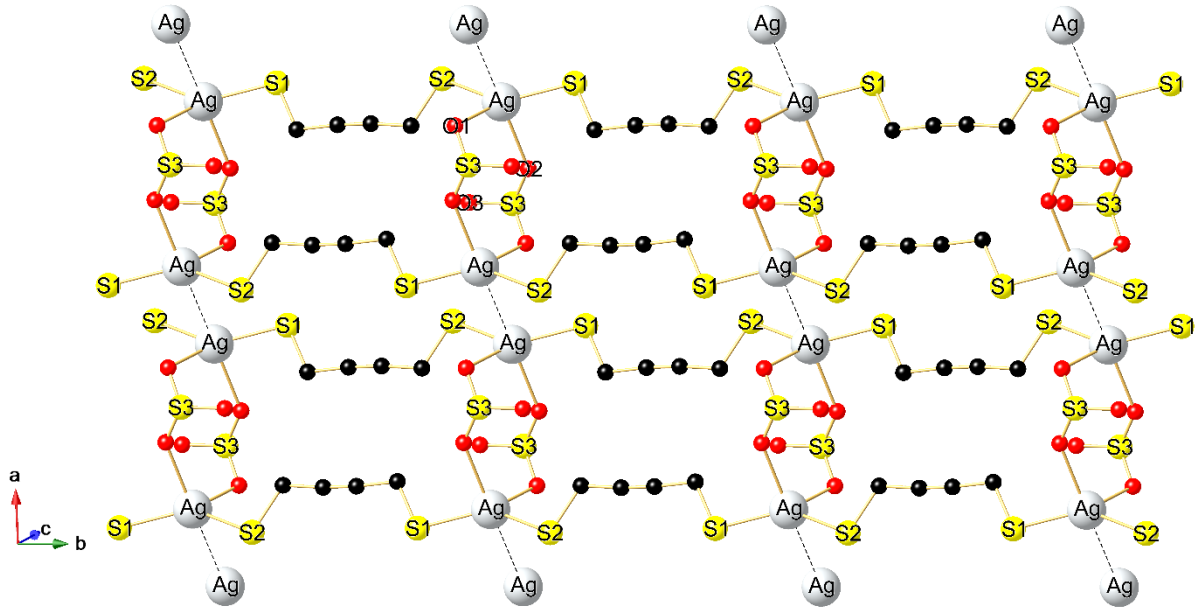

Figure 2. View of the 2D grid-like network of **CP1** (the phenyl and tosyl groups and the H atoms are omitted for clarity).

Structure of [Ag(L_{Cy})(OTs)]$_n$ CP2

The reaction of AgOTs with L_{Cy} using a 1:1 molar ratio in a mixture of methanol/chloroform (Scheme 1) led to the formation of **CP2** which, as **CP1**, crystallizes in the triclinic $P\bar{1}$ space group (Table S1). Contrary to **CP1**, the asymmetric unit in **CP2** contains only one L_{Cy} ligand, one silver atom and one tosylate (Figure S6). The coordination sphere of the silver atoms is identical in **CP1** and **CP2**. However, the bulkiness of the cyclohexyl groups now prevents the occurrence of Ag···Ag interactions ($d_{Ag\cdots Ag}$ = 4.7884(7) Å), thus **CP2** is a 1D coordination polymer (Figure 3). All the phenyl rings of the tosylate groups are oriented parallelly to each other's in the same ribbon. As can be seen in Figure S7, the phenyl rings also stack parallelly within two neighbored ribbons (torsion angles = 0°). In **CP2**, both the average Ag–S distance and the mean Ag–O distances are slightly shorter than for **CP1** and TAXXIA (2.4837 and 2.4556 Å, respectively).[39] The repeating unit consists, as for **CP1**, of a 22-membered $Ag_4(L_{Cy})_2O_4S_2$ parallelogram-shaped metallamacrocycle of same length (10.576 Å for **CP1**

and 10.580 Å for **CP2** but shorter width (5.439 Å for **CP1** and 4.788 Å for **CP2**) (see Figure S8). Indeed, in **CP1** the torsion angle Ag–O2–O1–Ag is equal to 9.1° while in **CP2**, the torsion angle Ag–O2–O1–Ag is larger, close to 96°.

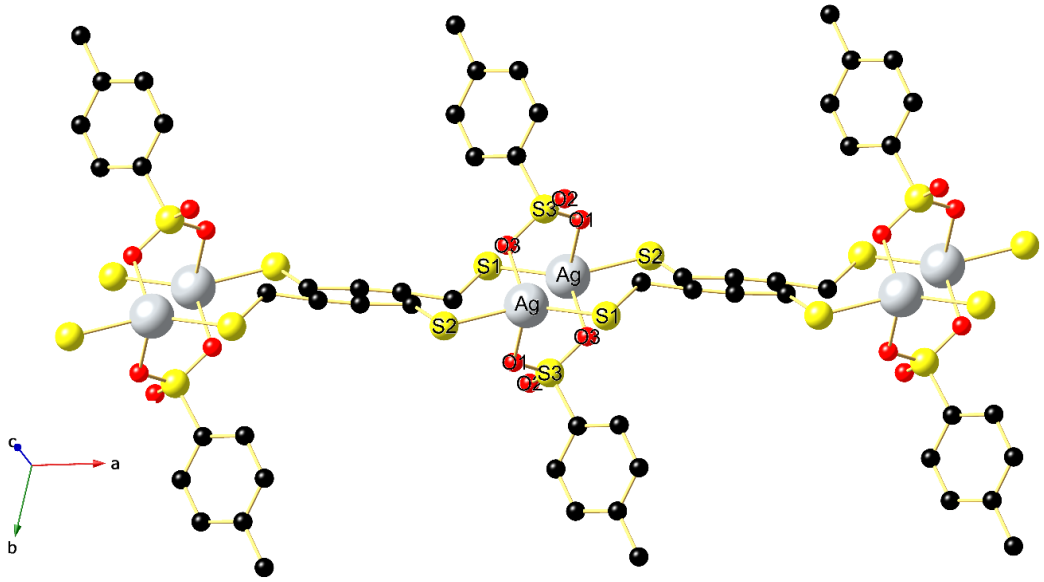

Figure 3. View of a segment of the 1D ribbon of **CP2** (the cyclohexyl groups and the H atoms are omitted for clarity).

Structure of [Ag(L_{tBu})(OTs)]$_n$ CP3

The reaction of AgOTs with L_{tBu} using a 1:1 molar ratio or a 2:1 ratio led invariantly to the same product (Scheme 1), **CP3** that crystallizes in the non-centrosymmetric orthorhombic $P2_12_12_1$space group (Table S1). The asymmetric unit in **CP3** contains two L_{tBu} ligands, two silver atoms and two tosylates (Figure S9). The 1D structure of **CP3** is reminiscent to the one of **CP2** (Figure 4). The phenyl rings in the 1D ribbon of **CP3** are, as in **CP2**, oriented parallelly but they are now tilted by 53° within two ribbons (Figure S10). The average Ag1–S distance in **CP3** is shorter than in **CP2** (2.4789 and 2.4837 Å, respectively) while the average Ag2–S distance is nearly similar (2.4843 Å). The mean Ag1–O and Ag2–O distances are analogous (2.466 and 2.465 Å). The $Ag_4(L_{tBu})_2O_4S_2$ metallamacrocycle is now 5.174 Å wide and 10.519 Å long. These dimensions are close to those of **CP1**, indeed the torsion angles Ag1–O1–O2–Ag2 and Ag1–O4–O5–Ag2 are equal to 7.7 and 5.4°, respectively.

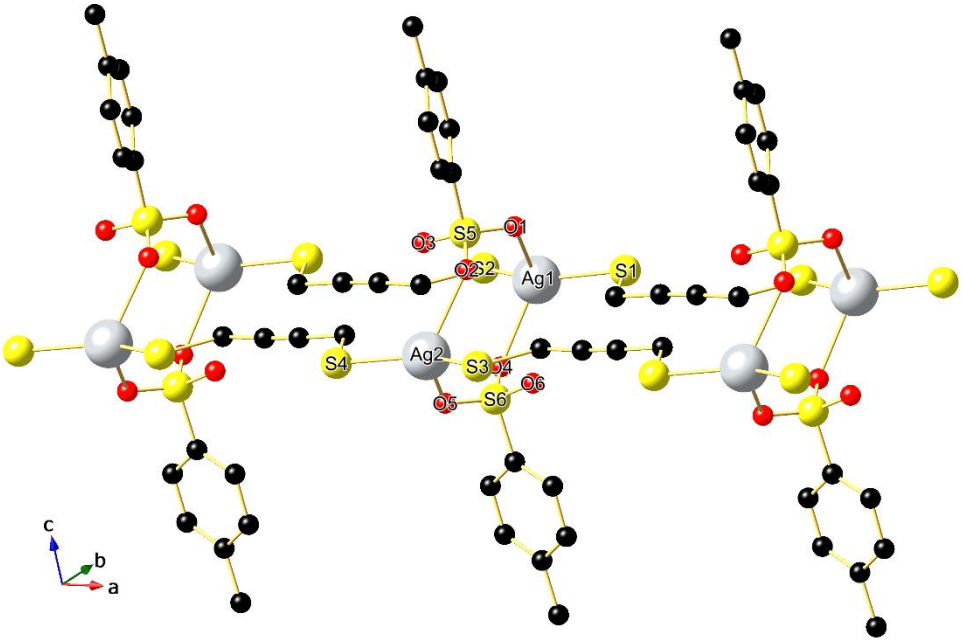

Figure 4. View of a segment of the 1D ribbon of **CP3** (the *tert*-butyl groups and the H atoms are omitted for clarity).

Coordination to silver triflate

Structure of the molecular complex $[Ag(L_{Ph})(OTf)]_2$ (D1)

For this second series, we aimed to study the impact of the nature of the sulfonate anion RSO_3^- on the CPs' architecture and switched from tosylate (R = *p*-Tolyl) to trifluoromethanesulfonate ($R = CF_3$). Unfortunately, using the same synthetical protocol, we failed to grow crystals from the 1:1 reaction of L_{Ph} with AgOTf ($AgCF_3SO_3$) in MeCN solution. However, we managed to obtain X-ray suitable crystals in good yield (78%) by a simple modification of the experimental procedure. For this, AgOTf dissolved in MeCN was allowed to diffuse into a dichloromethane solution of the ligand (Scheme 2).

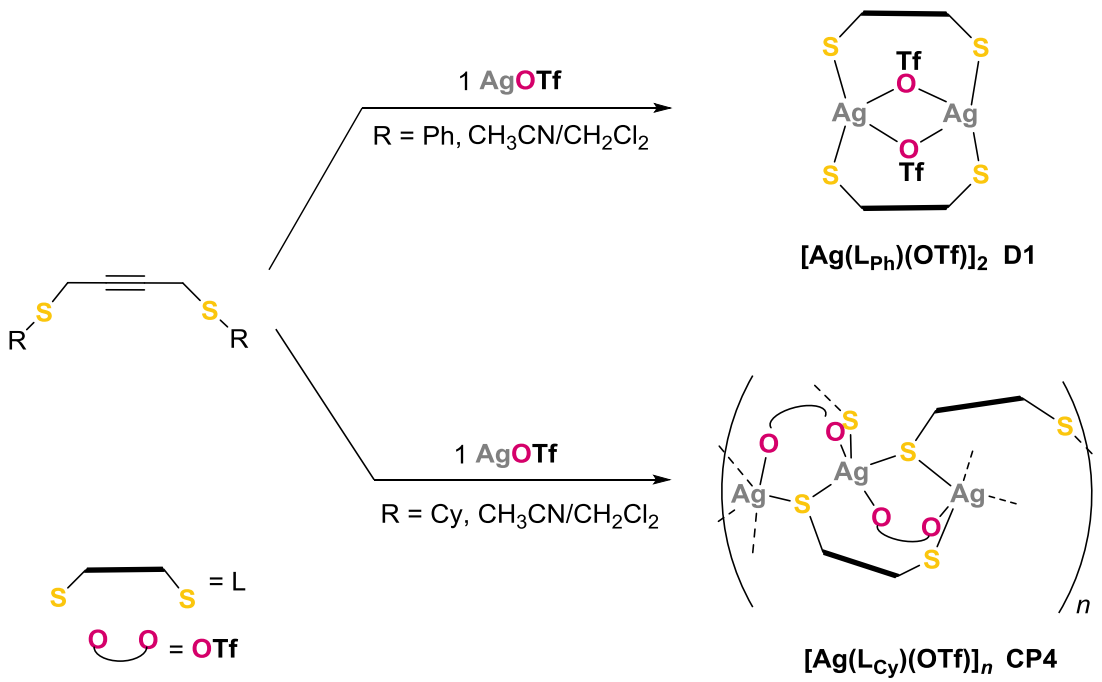

Scheme 2. Reaction of silver triflate (AgOTf) with L_{Ph} and L_{Cy} forming **D1** and **CP4**.

Surprisingly, analysis of the crystals revealed that not a targeted polymeric material was formed but a discrete dinuclear molecular species **[Ag(L_{Ph})(OTf)]$_2$** (**D1**). In the highly symmetric framework, each silver atom is four-coordinated in a distorted AgO2S2 tetrahedral environment (τ_4 = 0.81), constituted by two sulfur atoms from two different ligand molecules (Ag–S1 2.4888(8) Å; Ag–S2 2.4750(9) Å) and to two oxygen atoms from two triflate anions (Ag–O1 2.4472(19) Å and Ag–O1^1 2.4640(18) Å) (Figure 5). The triflate ions act as bridging ligands linking two Ag(I) centers via one oxygen atom in a μ_2-(κ^2O) coordination mode. The Ag···Ag separation of 3.909 Å precludes any interactions. The acetylenic dithioether ligand spans the two metal centers. Such coordination mode resembles the one obtained in the dinuclear [{Cu(μ_2-I)$_2$Cu}{μ-CySCH$_2$C≡CCH$_2$SCy)$_2$}].[35] This original coordination is due to the rigidity of the ligand featuring a linear CH$_2$-C≡C-CH$_2$ array preventing its coordination in a chelating mode. The structure of this complex is similar to the one found in [Ag$_2$(μ-dppb)$_2$(CF$_3$SO$_3$)$_2$] (dppb = bis(diphenylphosphino)butane)[40] with the dppb ligand also spanning the two metal centers. There are weak intramolecular hydrogen bonds between one of the sulfonate oxygen atoms O2 that is not engaged with the Ag(I) center and a hydrogen of the propargylic CH$_2$ group (*d*(H10B···O2) = 2.452 Å) and with one other hydrogen of the phenyl group (*d*(H12···O2) = 2.565 Å). There is also one C−H···F contact (*d*(H7B···F1) = 2.514 Å) (Figure S12). Intermolecular hydrogen interactions between neighboring dimers involving the non-coordinated sulfonate oxygen atoms O2 and O3 are observed with one

hydrogen of a thiophenyl group (d(H15···O2) = 2.498 Å) and with a hydrogen atom of a SCH_2 group adjacent to the triple bond (d(H7A···O3) = 2.594 Å). A survey of the Cambridge Structural Database (CSD) reveals that this complex constitutes the first example of coordination of dithioether ligands with silver triflate to form a dimer. The homogeneity of the product was also confirmed by PXRD. The simulated PXRD pattern matches well the experimental one (Figure S25).

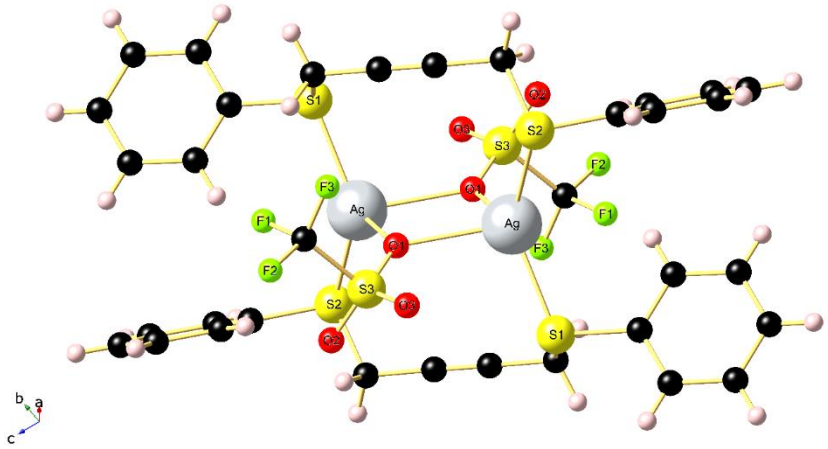

Figure 5. Molecular structure of **D1**.

Structure of [Ag(L_{Cy})(OTf)]$_n$ (CP4)

The outcome of the reaction that was performed under the same reaction conditions as for **D1** but using the sterically more crowded L_{Cy} is totally different (Scheme 2). Single-crystal diffraction analysis revealed the formation of a 1D polymer which crystallizes in the non-centrosymmetric orthorhombic $P2_12_12_1$ space group and having a **[Ag(L_{Cy})(OTf)]$_n$** composition (Table S2). The asymmetric unit of **CP4** is composed of one L_{Cy} ligand, one silver ion and one triflate anion (Figure S13). The silver center is five-coordinated to three S atoms of different ligands (d(Ag–S2^1) = 2.5282(6) Å, d(Ag–S1^2) = 2.6965(5) Å, and d(Ag–S1) = 2.5402(5) Å) and to two O atoms of distinct triflates in a AgS3O2 coordination mode (d(Ag–O1) = 2.5892(18) Å and d(Ag–O2) = 2.5905(16) Å). As expected, the average Ag–S and Ag–O distances are much shorter in the dimer complex **D1** than in **CP4**. The Ag ion adopts a distorted square pyramidal geometry with a $\tau5$ value of 0.33[41] (∠O1–Ag–O2 = 155.77(6)° and ∠S1–Ag–S1^2 = 135.643(10)°) and is placed 0.75 Å above the basal plane (defined by O1, S1, O2, S1^2). The ligand L_{Cy} adopts a dissymmetric μ_3-bonding mode (μ_3-(κ^2S^1:κ^1S^2) with S1 acting as a 4-electron donor and S2 acting as 2-electron donor. Triflate anions chelate two silver atoms in the same μ_2-(κ^1O^1:κ^1O^2) coordination mode as the

tosylate anions. However, in the case of **CP4**, only a single triflate anion bridges two Ag ions (Figures 6 and S14). As in **D1**, there are numerous intramolecular hydrogen bonding interactions. Noticeably, now the oxygen atoms coordinated to the silver centers are engaged in these interactions involving the hydrogen atoms of the cyclohexyl group (*d*(H12A···O2) = 2.467 Å, *d*(H6B···O1) = 2.461 Å) and a hydrogen of the propargylic CH2 group (*d*(H6A···O2) = 2.697 Å). There is also one intramolecular C−H···F contact (*d*(H7B···F3) = 2.524 Å) (Figure S15). Further weak intermolecular interchain interactions occur in the crystal between F2 and the propargylic CH_2 moiety (*d*(H10B···F2) = 2.604 Å) and between the uncoordinated oxygen of the triflate anion with the hydrogen atom of a cyclohexyl group of a neighboring CP (*d*(H16B···O3) = 2.694 Å) (Figure S15).

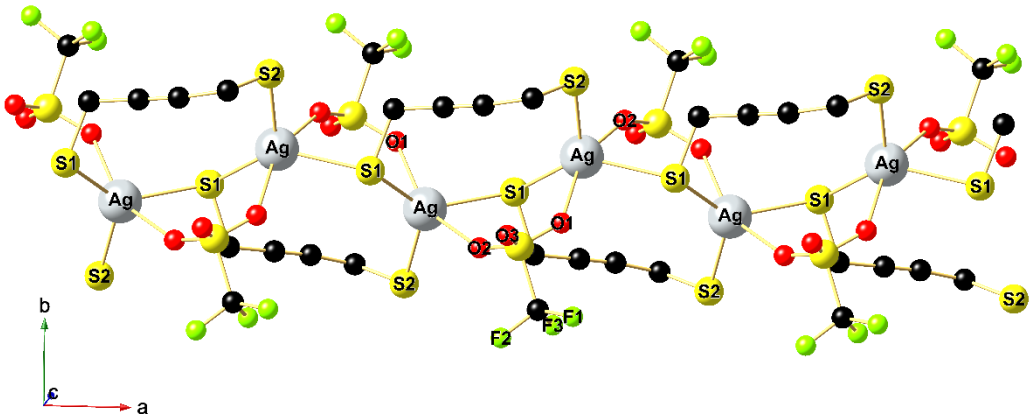

Figure 6. View of a segment of the 1D ribbon of **CP4** running along the *a* axis (the cyclohexyl groups and the H atoms are omitted for clarity).

Coordination to silver trifluoroacetate

Structure of $[Ag(L_{Cy})(CF_3CO_2)]_n$ (CP5)

In this last series, we kept the nature of the R group (CF_3) constant and switched from sulfonate to carboxylate anions. The reaction of $AgCF_3CO_2$ with 2 equivalents of L_{Cy} in acetonitrile affords **CP5** (Scheme 3).

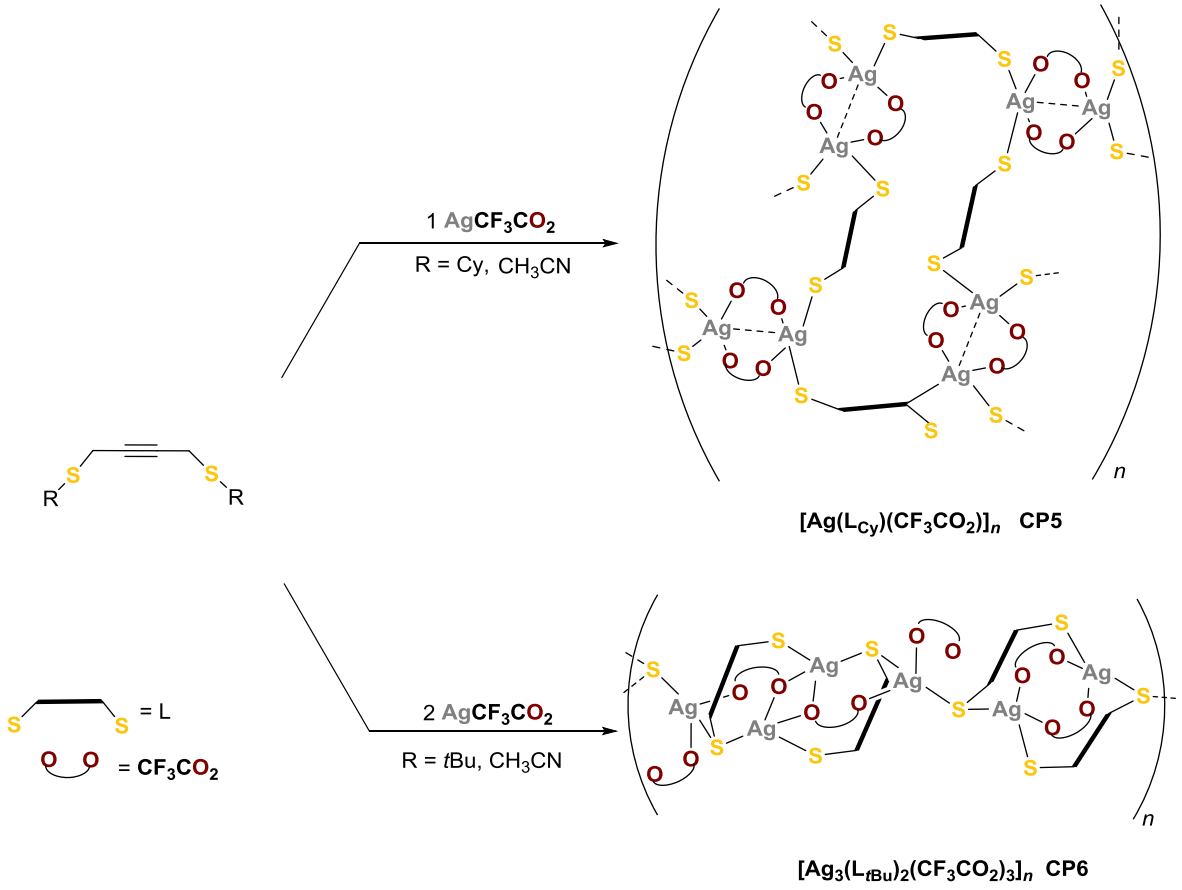

Scheme 3. Reaction of silver trifluoroacetate ($AgCF_3CO_2$) with L_{Cy} and L_{tBu} forming **CP5** and **CP6**.

X-ray suitable single crystals crystallizing in the monoclinic space group $P2_{1/c}$ were obtained by the slow evaporation of the solution. This product is a 2D CP of composition **[Ag(L_{Cy})(CF_3CO_2)]$_n$** *i.e.* a 1:1 metal-to-ligand ratio (Figures 7 and S16). We therefore repeated the reaction of L_{Cy} with $AgCF_3CO_2$ using a 1:1 ratio and obtained again **CP5** in very good yield (91%). **CP5** contains only one crystallographic type of silver atom. Two adjacent silver atoms are bonded together in a binuclear bridging mode with two trifluoroacetate anions to form a $Ag_2(CF_3CO_2)_2$ dimer (d(Ag–O1[1]) = 2.4428(10) Å, d(Ag–O2) = 2.4342(10) Å). The coordination sphere around Ag is completed by the coordination of two sulfur atoms stemming from different L_{Cy} ligands (d(Ag–S2[2]) = 2.5343(3) Å, d(Ag–S1) = 2.4758(3) Å). The Ag ion thus adopts a AgO2S2 coordination mode with a distorted tetrahedral geometry (τ_4 value of 0.68). Contrary to **CP2**, L_{Cy} is now not linking two dimers to form a 1D CP. The $Ag_2(CF_3CO_2)_2$ dimers are associated in **CP5** by four L_{Cy} ligands giving rise to the formation of a 2D polymer composed of 30-membered $Ag_6(L_{Cy})_4$ metallamacrocycles. 2D CPs have been described by Brisse's group upon the coordination of dithioether ligands (1,3-bis(phenylthio)propane, 1,2-bis(phenylthio)ethane) with $AgCF_3CO_2$.

In their case, the $Ag_2(CF_3CO_2)_2$ dimers are linked by two ligands to form 1D chains but each sulfur atoms are acting as 4-electron donor, so the chains are interconnected to form a 2D-CP.[39, 42] The Ag···Ag distance ($d_{Ag\cdots Ag}$ = 3.1601(2) Å), indicates the presence of supported argentophilic interactions.[38] Other examples of this coordination mode (AgO2S2 with bridging acetate) include 2D catena-((μ_4-1,3-bis(phenylthio)propane)-bis(μ_2-trifluoroacetato)-di-silver(I)) with $d_{Ag\cdots Ag}$ = 3.246 Å[39] (CSD ref code TAXWUL), the bis(μ_2-trifluoroacetato)-tetrakis(1,4,7-trithiacyclododecane-8,12-dione-S4)-di-silver(I) (CSD ref code CONJIZ)[43] with $d_{Ag\cdots Ag}$ = 3.785 Å, and the complex obtained by coordination of resorcinarene bis-thiacrown with $AgCF_3CO_2$ ($d_{Ag\cdots Ag}$ = 3.9341 Å) (LAKBEH).[44] This structure contains also some weak intramolecular hydrogen bonding interactions between the O2 atom of the trifluoroacetate and H11 of the cyclohexyl group (d(H11···O2) = 2.467 Å) and between O1 and the propargylic CH2 (d(H10A···O1) = 2.681 Å). One intermolecular hydrogen contact occurs between one of the fluorine atoms of the trifluoroacetate and one hydrogen atom of a nearest cyclohexyl group (d(H4B···F3A) = 2.609 Å) (Figure S18).

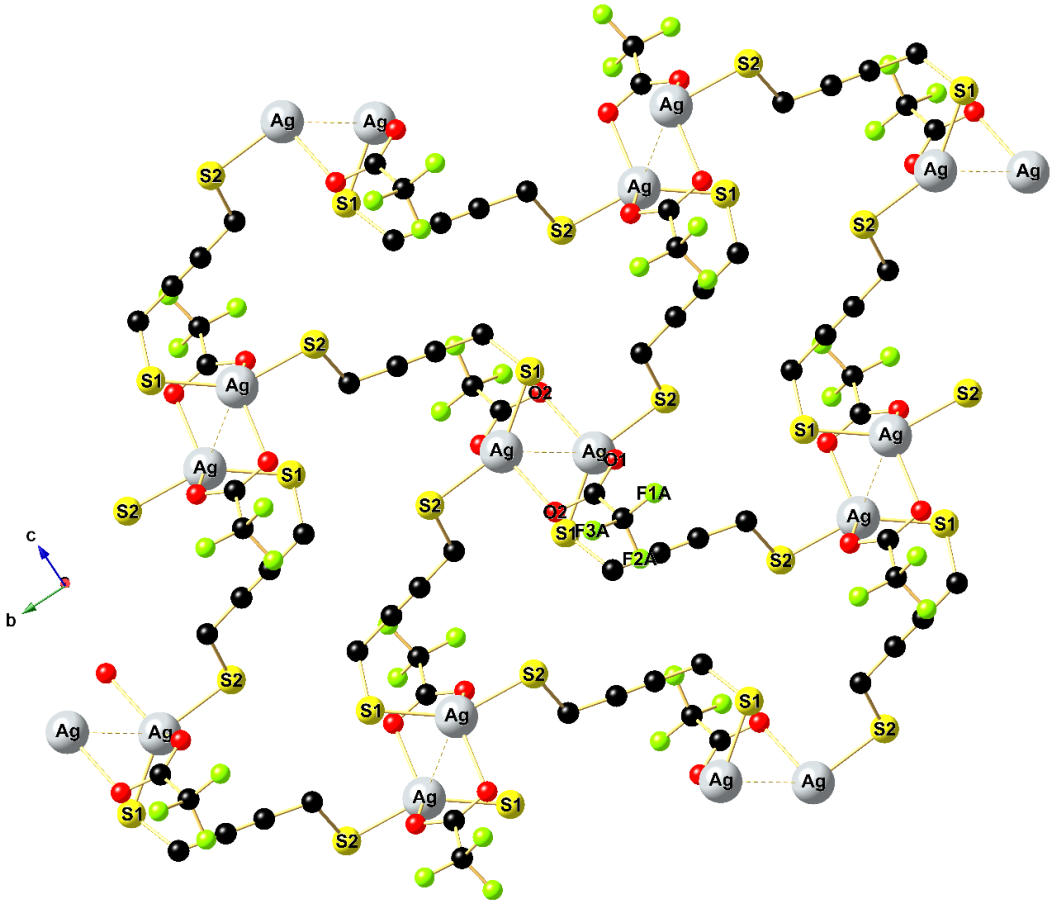

Figure 7. View down the *a* axis on a segment of the 2D layer of **CP5** (the cyclohexyl groups and the H atoms are omitted for clarity).

Structure of $[Ag_3(L_{tBu})_2(CF_3CO_2)_3]_n$ (CP6)

Under the same experimental conditions, the reaction of 1 equivalent L_{tBu} and 2 equivalents $AgCF_3CO_2$ affords a 1D CP crystallizing in the triclinic $P\overline{1}$ space group. The asymmetric unit contains three different silver atoms, three trifluoroacetate groups, and 2 different L_{tBu} ligands (Figures S19 and S20). The Ag3L2 composition was confirmed by elemental analysis. All Ag atoms are four-coordinated in an AgO2S2 distorted tetrahedral environment (τ_4(Ag1) = 0.78, τ_4(Ag2) = 0.82, τ_4(Ag3) = 0.70). **CP6** contains one bridged $Ag_2(CF_3CO_2)_2$ dimer formed with two centrosymmetrically related Ag3 atoms ($d_{Ag3\cdots Ag3}$ = 3.9029(5) Å) and two trifluorocarboxylate groups in a di-bridging mode (d(Ag3–O6A) = 2.429(3) Å, d(Ag3–$O5^2$) = 2.3957(14) Å) (Figure 8). The coordination sphere of the Ag3 center is completed by the coordination of two sulfur atoms of different ligands (d(Ag3–$S3^2$) = 2.6137(4) Å, d(Ag3–S4) = 2.5151(4) Å). **CP6** also contains a $Ag_4(CF_3CO_2)_4$ tetramer in which two Ag1 atoms are connected to each other's via one of the oxygen atoms O1 of two trifluorocarboxylate groups (d(Ag1–$O1^1$) = 2.4567(11) Å, $d_{Ag1\cdots Ag1}$ = 3.7285(4) Å). Each of the remaining O2 trifluorocarboxylate groups is coordinated to one Ag2 (d(Ag2–O2) = 2.4178(12) Å). Two L_{tBu} ligands are spanning these $(Ag1)_2$ dimers d(Ag1–S1) = 2.5200(4) Å, (d(Ag1–S2) = 2.4698(4) Å). One out of the two sulfur atoms of the ligands spanning the $(Ag1)_2$ and $(Ag3)_2$ dimers is acting as a four-electron donor and is also coordinated to Ag2 (d(Ag2–$S1^1$) = 2.5715(4) Å, (d(Ag2–S3) = 2.4974(4) Å), leading to the formation of a 1D CP. The coordination sphere of Ag2 is completed by the coordination of one oxygen atom of a trifluorocarboxylate anion (d(Ag2–O3) = 2.2981(13) Å). This structure presents also numerous C−H···O and C−H···F contacts (Figure S21), the stronger ones being observed between (*i*) the oxygen atoms of the trifluoroacetate and (*ii*) the hydrogen of the propargylic CH_2 (d(H21B···O4) = 2.234 Å), (d(H5B···O5) = 2.386 Å), (*iii*) the hydrogen of the tert-butyl group (d(H2C···O3) = 2.467 Å) and between one fluorine of the CF_3 and finally an hydrogen atom of the tertbutyl group (d(H4A···F7) = 2.590 Å). The sum of all these secondary interactions is generating a 3D supramolecular network.

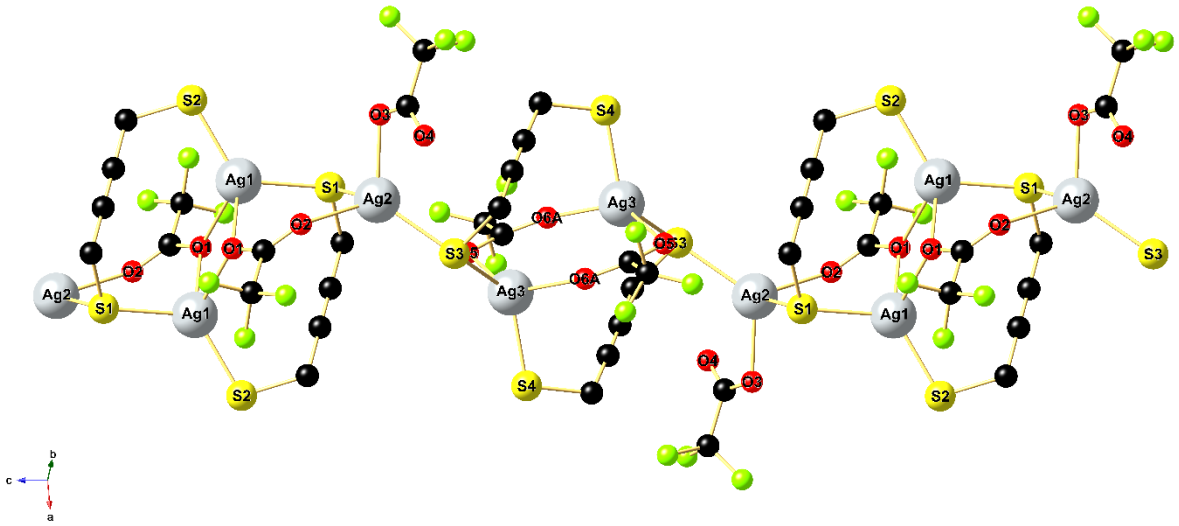

Figure 8. View of a segment of the 1D ribbon of **CP6** running along the *c* axis (the tert-butyl groups and the H atoms are omitted for clarity).

Discussion on the principal differences between the structural parameters.

Table 1 summarizes selected structural parameters of the obtained CPs. Whatever the ligand (L_{Ph}, L_{Cy} and L_{tBu}), the coordination with silver tosylate led to the formation of CPs with the same tetrahedral AgO2S2 coordination environment around the metal center. In these compounds, two tosylate anions act as bridging ligands through two oxygen atoms coordinating two silver ions. The resulting dimer forms an eight-membered $Ag_2O_4S_2$ metallacycle. The coordination of the dithioether ligands in a μ_2 bridging mode to the silver centers led to the formation of a double Ag–S—S–Ag 1D chain joining the dimeric $Ag_2O_4S_2$ units and generating a second 22-membered $Ag_4L_2O_4S_2$ metallamacrocycle. It produces a ladder-like 1D polymer. In **CP1**, adjacent double chains are linked together via Ag···Ag interactions responsible for the formation of a 2D network. The tosylate anions thus do not play a decisive role in directing the formation of the polymeric network.

Replacement of the *p*-tolyl by a trifluoromethyl group allows to achieve a wider diversity regarding the dimensionality, the ligand and anions coordination mode and the Ag(I) geometry. A molecular centrosymmetric dimer is obtained with L_{Ph} while a polymer chain results from the coordination of the L_{Cy} ligand. Two triflate units bridge symmetrically two silver ions through a single oxygen atom as a four electrons donor in **D1** creating a 4-membered cycle Ag_2O_2. In **CP4**, two consecutive Ag centers are connected through a sulfonate group in a bidentate coordination mode yielding a strand $(AgOSO)_n$. In **D1**, the coordination of the L_{Ph} ligands in a symmetric μ2 bridging mode to silver ions led to the

dimeric entity Ag_2L_{Ph2}. The dithioether L_{Cy} ligand adopts a dissymmetric bridging coordination mode with a sulfur intercalated between two neighboring Ag(I) and acting as a four-electrons donor. The second S atom is singly coordinated to the adjacent silver center. The resulting cyclic units $Ag_2L_{Cy}S$ are connected via a common AgS bond giving rise to a 1D ribbon which is developed in the same direction as the $(AgOSO)_n$ strand. These different bonding modes of the ligands and anions in **D1** and **CP4** imply a silver tetrahedral geometry AgO_2S_2 in **D1** and a silver square pyramidal arrangement AgO_2S_3 in **CP4**.

The structural organization is also variable using the trifluoroacetate anion. A dimer $Ag_2(O_2CCF_3)_2$ resulting from a μ_2-O,O' bonding mode featuring an additional Ag···Ag interaction is observed in **CP5**. A similar bis-bidentate bonding of the anion occurs in **CP6** and gives rise to a centrosymmetric dimer involving Ag3. Another centrosymmetric tetrameric unit $Ag_4(O_2CCF_3)_4$ is also present. This tetramer is formed with two bridging trifluoroacetate bonding four silver ions (two Ag1 and two Ag2) through (i) an oxygen atom O1 acting as a four-electrons donor creating a 4-membered cycle Ag_2O_2 (ii) a second oxygen O2 being a 2-electron-donor which links the Ag_2O_2 cycle to two other Ag centers. The latter are also coordinated to one oxygen atom of another CF_3CO_2 group. In **CP5**, the coordination of the L_{Cy} ligands in a μ_2-S,S' bridging mode to silver ions associate four dimer units $Ag_2(O_2CCF_3)_2$ generating 30-membered $Ag_6(L_{Cy})_4$ metallamacrocyles which are interconnected leading to a 2D herringbone layer. In **CP6**, a dissymmetric bridging coordination mode is observed for the dithioether L_{tBu} ligands with a 2- and a 4-electron donor S atom completing the tetrahedral AgO2S2 coordination environment around the metal centers. The L_{tBu} ligand bridges the silver centers of the tetrameric unit $Ag_4(O_2CCF_3)_4$ creating a bigger tetramer $Ag_4(O_2CCF_3)_4(L_{tBu})_2$. The Ag3 atoms of the dimer $Ag_2(O_2CCF_3)_2$ are also spanned by 2 ligands and the 4-electron donating sulfur atom S3 are connected to Ag2 centers from the tetramer leading to a 1D polymer $(tetramer\text{-}S\text{-}dimer\text{-}S)_n$. This series of CPs resumed in Table 1 illustrates the structural richness obtained upon coordination of silver with semi-rigid dithioether ligands and oxygenated anions.

Table 1. Structural comparison of the CPs.

Formula	CP	Dimensionality	Ag^{I} geometry	Ligand coordination mode	Average Ag–S length (Å)	Average Ag–O length (Å)	*d*(Ag···Ag) (Å)
$\mathbf{[Ag(L_{Ph})_{1.5}(OTs)]_n}$	**CP1**	2D	Tetrahedral AgO2S2	μ2	2.514	2.467	3.2242
$\mathbf{[Ag(L_{Cy})(OTs)]_n}$	**CP2**	1D	Tetrahedral AgO2S2	μ2	2.484	2.457	
$\mathbf{[Ag(L_{tBu})(OTs)]_n}$	**CP3**	1D	Tetrahedral AgO2S2	μ2	2.482	2.465	
$\mathbf{[(Ag(L_{Ph})(OTf)]_2}$	**D1**	0D	Tetrahedral AgO2S2	μ2	2.482	2.456	
$\mathbf{[(Ag(L_{Cy})(OTf)]_n}$	**CP4**	1D	Square-based pyramidal AgO2S3	μ3	2.588	2.599	
$\mathbf{[(Ag(L_{Cy})(CF_3CO_2)]_n}$	**CP5**	2D	Tetrahedral AgO2S2	μ2	2.505	2.439	3.1601
$\mathbf{[(Ag_3(L_{tBu})_2(CF_3CO_2)_3]_n}$	**CP6**	1D	Tetrahedral AgO2S2	μ3	2.532	2.391	

Infrared spectroscopy

The strong broad bands at 1006-1186 cm^{-1} found for **CP2** and **CP3** can be assigned to the stretching vibrations of the tosylate anion.[45] These bands are less visible in **CP1** due to the presence of an excess of the L_{Ph} ligand. **D1** and **CP4** also present intense bands in the 1000-1300 cm^{-1} range due to the presence of SO_3 and CF_3 vibrations.[46] In **CP5** and **CP6**, the presence of the trifluoroacetate anions was confirmed by the observation of bands at ≈1653 cm^{-1} and at ≈1400 cm^{-1} attributed to the $\nu_{as}(COO)$ and $\nu_s(COO)$ respectively.[47] In these compounds, strong bands are also observed in the 1120-1170 cm^{-1} range due to the stretching vibrations of CF_3. In **CP6**, all these bands are split due to the presence of different coordination modes of the trifluoroacetate anions. In the 514-523 cm^{-1} fingerprint range an additional band was observed for **D1**, **CP4**-**CP6** confirming the presence of C−H···F hydrogen bonds.[48]

Stability and thermal analyses

Although silver complexes are known for their luminescence properties that are significantly influence by argentophilic interactions,[49] none of these CPs was luminescent at room temperature. All compounds were however found to be stable over several months when stored in the dark in the fridge. This absence of aging was confirmed by measuring their PXRD at different time intervals (Figures S22-S28). The thermal stabilities of all compounds were studied by TGA under a nitrogen flow in the temperature range 20-850°C. Figure 9 summarizes all TGA traces while all first derivatives plot of the TGA traces can be found in

ESI (Figures S29-S35). The values of thermal stabilities Td_5 (corresponding to 5% weight-loss) are given in Table 2. The dimer **D1** presents the highest thermal stability with Td_5 = 232°C while **CP5** and **CP6** containing CF_3CO_2 anions decompose at 144 and 129°C, respectively. Then, for a same tosylate anion, the thermal stability followed the order **CP2** (204°C) ≈ **CP1** (193°C)> **CP3** (161°C). As the coordination of the anions around the silver center and the dimensionality are the same in **CP1-CP3** (if the Ag···Ag interactions are neglected), this difference in thermal stability can be explained by the nature of the S-R group. We thus consider that, upon thermal treatment, both the anions and the S-R groups decomposed. Based on this hypothesis, we found a good matching between the theoretical and experimental residual values for all our compounds. As observed for Cu-based CPs incorporating these dithioether ligands, the difference in thermal stabilities for **CP1**-**CP2** *vs* **CP3** can be attributed to differences in the boiling point of cyclohexyl mercaptan (158°C) and phenyl mercaptan (169°C) versus *tert*butyl mercaptan (65°C).[35] For this reason also, the thermal stability of **CP6** is lower than that of **CP5**.

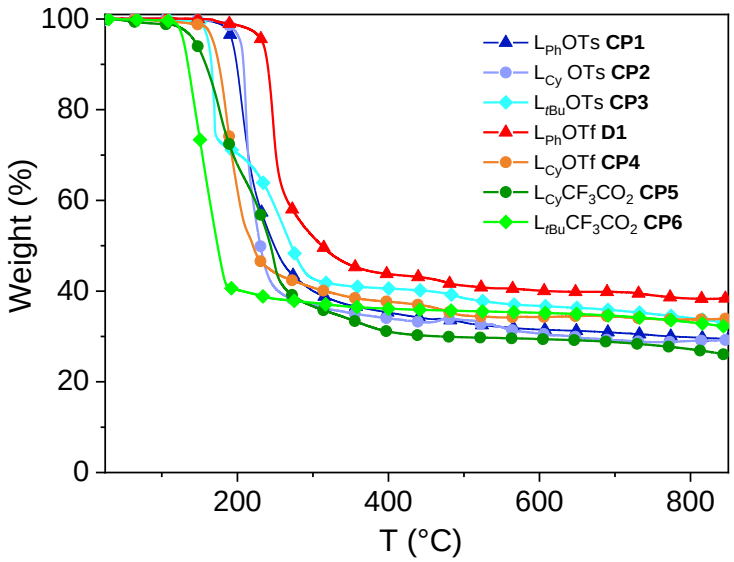

Figure 9. TGA traces of all compounds measured under nitrogen flow (rate: 10°C/min).

Table 2. TGA data of all compounds.

	$L_{Ph}OTs$ **CP1**	$L_{Cy}OTs$ **CP2**	$L_{tBu}OTs$ **CP3**	$L_{Ph}OTf$ **D1**	$L_{Cy}OTf$ **CP4**	$L_{Cy}CF_3CO_2$ **CP5**	$L_{tBu}CF_3CO_2$ **CP6**
Td_5 (°C)	193	204	161	232	168	144	129
Theo res[a] (wt%)	27.2	28.5	31.4	30.4	29.6	31.7	38
Exp res	29.5	29.2	33.1	38.4	33.9	26	32

(wt%)

[a] values determined based on anions and S-R thioether part loss.

Antibacterial activities

The antibacterial activities of all CPs were investigated against Gram-negative bacteria, *E. coli* and Gram-positive bacteria, *S. aureus*, chosen as model microorganisms. Before the measurements, we checked the homogeneity of all samples by powder X-ray diffraction (PXRD) and the experimental diffractograms were compared with the simulated ones obtained from the single crystals (Figures S22-S28). MIC values (corresponding to the lowest concentration of a chemical with no visible bacterial growth) of all CPs were determined in suspension in culture media. Indeed, we have shown previously that the solubilization of this kind of CPs in water/DMSO solutions (95/5% v/v) led to the disruption of the CP releasing silver ions and free ligands.[34] From the results of Table 3, three groups can be considered. The first one contains **CP1**, **CP2**, **CP3** and **D1** with comparable MICs against *E. coli* in the 16-20 µg Ag per mL range and against *S. aureus* in the 10-20 µg Ag per mL range. These values are in the same range as those we have previously reported.[34] **CP4** is a little on the fringes of this first group with slightly higher MIC and minimal bactericidal concentration (MBC) values against both bacteria. The third group includes CPs with trifluoroacetate anion (**CP5** and **CP6**) that show the highest antibacterial activity with MIC values in the range 5-10 and 2-8 µg Ag per mL against *E. coli* and *S. aureus*, respectively. All CPs present however close MIC and MBC values showing that they present both bacteriostatic and bactericidal activity. At the same time, the free ligands do not present any antibacterial activity in the studied concentration range. A comparison with MIC values of other CPs described in the literature is a difficult task since generally the MICs are not expressed in µg Ag per mL but rather in µg/mL or µmole/mL of compound and some CPs were firstly dissolved in DMSO.[50, 51] We also checked that the nature of the counter-anion of the silver salts has no significant influence on the antibacterial properties by measuring MICs values of $AgCF_3CO_2$ and AgOTs and found similar values (see Table 3). From these observations, we can conclude that the differences in MIC values observed between the CPs are neither related to the nature of the ligand nor that of the counter-anions. It is generally admitted that the antibacterial activity of silver-containing CPs or MOFs can be related to a slow release of silver ions in solution.[52] To explain the differences observed in terms of MIC values between the CPs, we measured the amount of silver released from three CPs into a phosphate-buffer saline (PBS) solution after a 24 hours-contact by Inductively Coupled Plasma Atomic Emission Spectrometry (ICP-AES). We chose **CP2** $L_{Cy}OTs$, **CP3** $L_{t\mathrm{Bu}}OTs$ and **CP6** $L_{t\mathrm{Bu}}CF_3CO_2$ as **CP2** and **CP3** have similar

MIC values while **CP6** presents the lowest MIC. For these experiments, a starting concentration of CP equivalent to 16 µg Ag per mL, close to the MICs of **CP2** and **CP3** was used. After 24 hours, the amounts of silver released were equal to 0.16 µg Ag per mL for **CP2**, 0.56 µg Ag per mL for **CP3** and 0.33 µg Ag per mL for **CP6**. Thus, the most antibacterial efficient CP (**CP6**) does not release the highest amount of silver ions and CPs with the same MIC values (**CP2** and **CP3**) do not release the same silver content. Identical observations have already been made by other authors without being discussed.[53,21] Lee and collaborators have prepared antibacterial Cu-based MOFs and also obtained similar MICs but different Cu(II) release contents. They explained this discrepancy by the fact that Cu(II) ions were not only bactericidal but their Cu-MOFs themselves could participate in inactivating bacteria.[54]

Table 3. MIC and MBC values (expressed in µg Ag per mL) for all CPs, ligands and silver salts.

	***E. coli* ATCC 25922**		***S. aureus* ATCC 25923**		**Ag release[a] PBS 24h (µg per mL)**
	MIC	**MBC**	**MIC**	**MBC**	
L_{Ph} (6% vol MeCN)	> 80	nd	> 80	nd	-
L_{Cy} (6% vol MeCN)	> 80	nd	> 80	nd	-
L_{tBu} (6% vol MeCN)	> 80	nd	> 80	nd	-
$AgCF_3CO_2$	10-16		8-10		-
AgOTos	10-16		5-8		-
CP1 L_{Ph}OTs	16-20	20-32	16-20	32-40	-
CP2 L_{Cy}OTs	16-20	16-20	16-20	32-40	0.16
CP3 L_{tBu}OTs	16-20	16-20	10-16	16-20	0.56
D1 L_{Ph}OTf	16-20	16-20	16-20	20-32	-
CP4 L_{Cy}OTf	32-40	64-80	32-40	32-40	-
CP5 $L_{Cy}CF_3CO_2$	8-10	8-10	2-2.5	2-2.5	-
CP6 $L_{tBu}CF_3CO_2$	5-8	10-16	5-8	5-8	0.33
$L_{Ph}NO_3$[34]	20	20	10	10	
$L_{Cy}NO_3$[34]	20	40	10	10	
Silver(I) sulfadiazine[55]	5-9.6		20-38		-

[a] using a starting CPs concentration of 16 µg per mL

Other parameters that can affect the antibacterial performances/silver release are the crystals' morphology and size. Therefore, the morphology of all our CPs was investigated by scanning electron microscopy (SEM) (Figure 10). In the tosylate series, **CP1** and **CP3** present a larger crystal size than **CP2**, the morphology of **D1** and **CP4** is rather similar and **CP6** possesses the biggest crystals. Intuitively, the larger crystals should release the lowest amount of silver.

Thus again, the difference in morphology could not explain the different MIC values obtained. We also took crystals of **CP3**, grinded them carefully and measured the amount of silver released over 6 hours in a PBS solution at 30° C. Figures S36 clearly shows a different morphology for both samples (**CP3** and **CP3 grinded**) but despite this difference, the amount of released silver remained nearly equal (0.222 and 0.195 µg per mL).

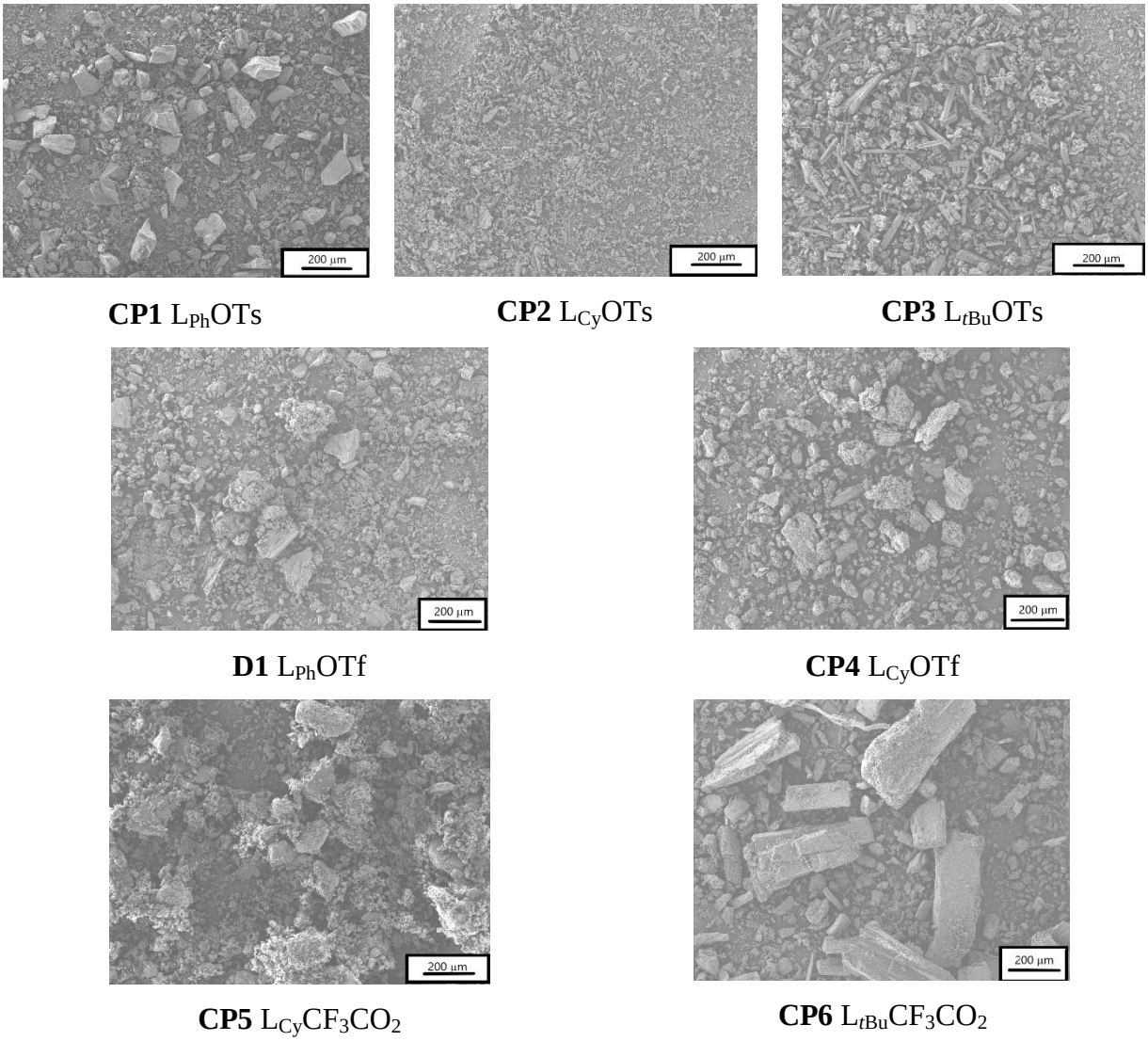

CP1 $L_{Ph}OTs$ **CP2** $L_{Cy}OTs$ **CP3** $L_{tBu}OTs$

D1 $L_{Ph}OTf$ **CP4** $L_{Cy}OTf$

CP5 $L_{Cy}CF_3CO_2$ **CP6** $L_{tBu}CF_3CO_2$

Figure 10. SEM images of all CPs.

Faced with this surprising result, we repeated the silver release experiments with all CPs (Figure 11.A) and measured at the same time their bactericidal activity by time-killing assays (Figure 11.B). These antibacterial measurements were performed in 100% PBS. Our previous study with nitrate-containing CPs have shown that, at concentrations closed to the MIC, the

bacteria were killed very quickly in about one hour whatever the nature of the CP. However, using a concentration of 1 µg Ag per mL we were able to make a clear correlation between the amount of silver released and the antibacterial properties.[34] We thus chose to work at this concentration. As can be seen in Figure 11, and contrary to what is observed for MICs, there is a good correlation between the amount of liberated silver and the rate of antibacterial efficiency. **CP3** containing the tosylate anion and the L_{tBu} ligand releases the highest quantity of silver (in accordance with the results discussed above) and kills the bacteria within 1 hour. Parallelly, **D1** delivers the lowest amount of silver and is the less efficient product. The second CP that liberates the highest amount is **CP6**, killing the bacteria within two hours. One of the objectives of this work was to establish a link between antibacterial efficiency and chemical structure. This is a challenging task as our CPs present different dimensionalities, silver coordination modes and counter anions binding mode. Interestingly, **CP2** and **CP3** adopt quite similar architectures allowing a comparison. As mentioned before, **CP3** releases the highest silver amount (0.27 µg Ag/mL) while, within the same time, **CP2** releases nearly an amount three time less (0.10 µg Ag/mL) and the bacteria are not entirely killed after 3 hours. From these observations, we can conclude that a clear correlation between chemical structure and silver released/antibacterial activity is difficult.

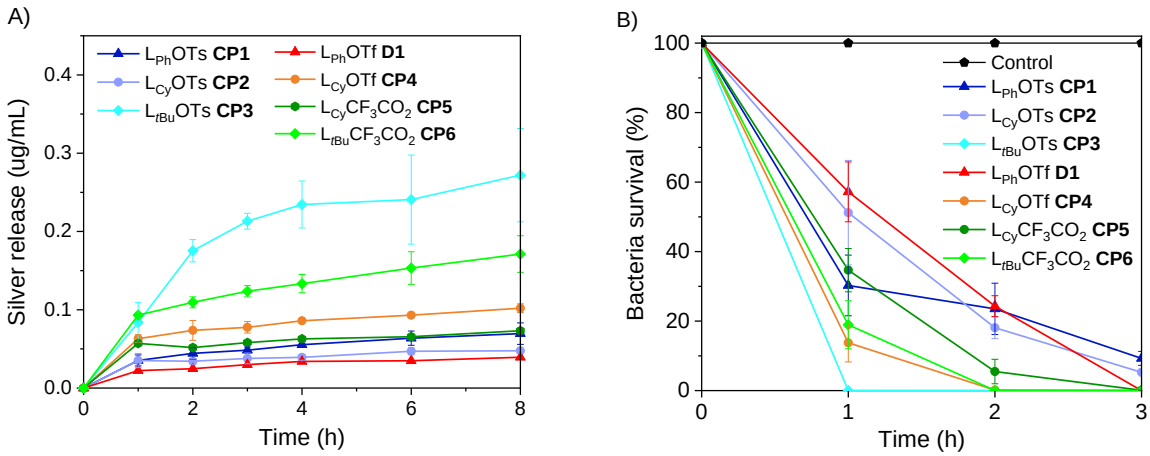

Figure 11. A) Silver released from all compounds in PBS at 30°C. B) % of surviving *E. coli* bacteria in PBS in the presence of all compounds at a concentration of 1 µg Ag per mL.

Cytotoxicity measurements

The *in vitro* cytotoxicity of all CPs has been estimated on normal human dermal fibroblasts (NHDF, cells within the dermis layer of skin which are responsible for generating connective tissue and allowing the skin to recover from injury). The cells were exposed to eight different

CPs concentrations which encompass MIC values (160, 80, 40, 20, 10, 5, 2.5, 1.25 μg/mL Ag) for 24 hours, followed by a viability assay (MTT for 3-(4,5-dimethylthiazol-2-yl)-2,5-diphenyltetrazolium bromide). Figure 12 summarizes the results of LD_{50} (lethal dose for 50% of the cells) for each CP and visualizes the results of microscopic observation. All other images and results of cell viability with various concentrations can be found in SI (Figures S38-S44). There is clearly no link/correlation between MICs and LD_{50} values. For **CP3**, no cells growth was observed in the concentration range used and is thus highly cytotoxic. On the other hand, **CP2** and **CP5** present LD_{50} values of 77 and 48 μg Ag/mL. These values are higher than their MIC ones and can thus be considered as biocompatible. **CP1** and **D1** have LD_{50} values that are too close to their MIC to be considered as biocompatible. For **CP4**, the therapeutic window is very narrow. The highest LD_{50} values were obtained with the CPs containing the L_{Cy} ligand (most potent) and the lowest LD_{50} values were obtained with the CPs with L_{tBu} ligands. At this moment, we have no explanation to rationalize this finding. Moreover, we found that the two highest LD_{50} values were obtained with the CPs that are releasing the highest amount of silver (**CP3** and **CP6**). Thus, the cytotoxicity could be related to the silver release. To investigate whether the decrease in cell viability could be due to necrosis, we measured the released of lactate dehydrogenase (LDH, an enzyme catalyzing the conversion of pyruvate to lactate and back, as it converts vice-versa NAD^+ to NADH) from damaged or destroyed cells in the extracellular fluid. Comparison with the absorbance values of the blank revealed no LDH released with our CPs (results not shown), thus the decrease in cell viability in our case is very probably due to apoptosis as observed in silver-based sol-gel coatings.[56]

	LD_{50}	**MICs**
CP1 $L_{Ph}OTs$	19	16-20
CP2 $L_{Cy}OTs$	77	16-20
CP3 $L_{tBu}OTs$	<1	16-20
D1 $L_{Ph}OTf$	21	16-20
CP4 $L_{Cy}OTf$	46	32-40
CP5 $L_{Cy}CF_3CO_2$	48	8-10
CP6 $L_{tBu}CF_3CO_2$	14	5-8

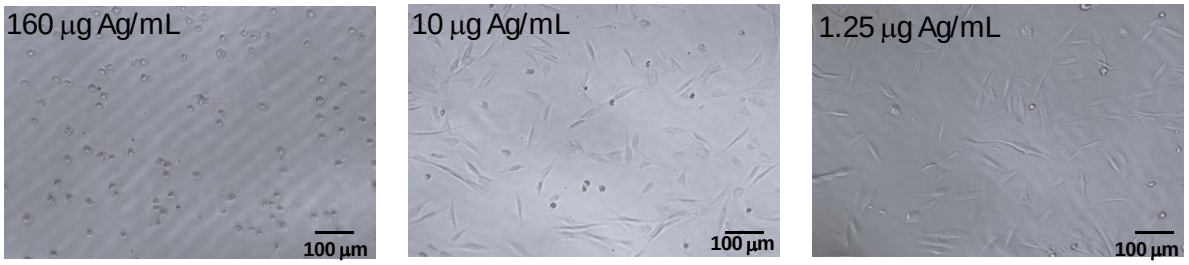

Figure 12. Values of lethal dose LD_{50} (lethal dose for 50% of the fibroblasts after a 24h exposure) with MICs (in µg Ag per mL) for all CPs. Examples of microscopic observations of the fibroblasts after 24h growth in the presence of various concentrations of **CP2**.

Conclusion

Antibacterial CPs were prepared by a straightforward self-assembly process of acetylenic dithioether $RSCH_2C{\equiv}CCH_2SR$ ligands with various Ag(I) salts. The coordination of these rigid ligands (R = Ph, Cy, *t*Bu) with silver tosylate, triflate, and trifluoroacetate led to the formation of 1D ribbons, 2D networks and a macrocyclic molecular complex in the case of **D1**. In five of out of six compounds, the silver ion is centered in a tetragonal environment and for the last one a square pyramidal geometry is crystallographically evidenced. These CPs present also various coordination mode of both the ligands and the oxygenated anions. Although examples of a π-coordination of acetylenic triple bonds to Ag(I) are literature-known, this kind of interaction was not observed for our materials.

Investigation of the antibacterial properties by MIC determination evidences good antibacterial efficiency against Gram-positive *S. aureus* and against Gram-negative *E. coli* for all CPs. However, our experiments reveal that a structure-activity-relationship (SAR) correlation between the amount of released silver and the chemical architecture is difficult to establish. Although we found that silver liberation could be correlated to the rapidity of the bactericidal action, the amount of silver released could not be correlated to MIC values. Thus, another parameter should play a role to achieve the antibacterial action. Nevertheless, the cytotoxicity can be related to the silver release. Indeed, the CPs that deliver the highest amount of silver are the more cytotoxic. Interestingly, in our study, three out of the six CPs were found to be biocompatible.

To summarize, we have demonstrated that the strategy consisting in strengthening the Ag-ligand bonding by association of soft-donor dithioether ligands with soft Lewis acid Ag(I) salt is efficient to prepare antibacterial materials with controlled silver release. This is a key point for biomedical applications to work in the therapeutic range. Also, our study raises the question whether the strategies developed by other laboratories consisting in the elaboration of water-soluble CPs or CPs able to release a high amount of silver, are valuable.

Experimental section

Materials and methods

1- Chemicals

Silver *p*-toluenesulfonate (AgOTs), silver triflate (AgOTf), silver trifluoroacetate ($AgCF_3CO_2$), NaOH, 1,4-dichlorobut-2-yne, *tert*-butylthiol, cyclohexanethiol, thiophenol, the culture media Mueller Hinton (MH) broth, Lysogeny broth Miller (Luria-Bertani), Microbiology Agar, the cell medium (Dulbecco's modified Eagle's medium (DMEM), 2% glutamine), trypsin EDTA (0.25-0.002%), tryptan blue, fetal bovine medium and PBS were commercially obtained from Acros, Alfa Aesar, Merck, Fischer, Aldrich, TCI and Difco.

2- Physical Measurement and Instrumentation.

The ^{1}H and $^{13}C\{^{1}H\}$ NMR spectra were recorded on a Bruker AVANCE 400 HD instrument with ^{1}H chemical shifts (ppm) referenced to the proton impurity of the NMR solvent and ^{13}C chemical shifts to the NMR solvent. Infrared spectra were recorded with a 2 cm^{-1} resolution on a Bruker vertex70 FTIR spectrometer using a Platinum ATR accessory equipped with a diamond crystal. Thermogravimetric analysis (TGA) was carried out on a TA Instruments Q600 in an alumina crucible under a nitrogen flow with a heating rate of 10 °C min^{-1} up to 850 °C. Inductively Coupled Plasma Atomic Emission Spectrometry (ICP-AES) measurements were performed on a Radial ICAP 6500 Model, Thermo Fisher Scientific (Courtaboeuf, France). The morphology of the CPs was obtained using a high-resolution scanning electron microscope MIRA3 TESCAN with an electron beam energy of 5 kV.

3- Synthesis

Ligand Synthesis

The dithioether ligands 1,4-bis(phenylthio)but-2-yne L_{Ph} and 1,4-bis(cyclohexylthio)but-2-yne L_{Cy} were synthesized in one step according to our previously reported protocol.[34]

Synthesis of L_{tBu} 1,4-bis(tert-butylthio)but-2-yne

tert-Butylthiol (5.59 g, 62 mmol) was added to a solution of NaOH (2.5 g, 62 mmol) in ethanol (140 mL) before cooling down to 0°C. 1,4-dichlorobut-2-yne (3.69 g, 30 mmol) was then slowly added and the mixture was stirred overnight at room temperature. The mixture was stirred overnight at room temperature. The NaCl precipitate was filtrated, the solvent was removed under vacuum and the product was dissolved in CH_2Cl_2. The organic phase was washed several times with water until silver nitrate test indicated that NaCl was fully removed. The resulting organic phase was then dried over Na_2SO_4, filtered, and the solvent was removed under vacuum. The residue was purified by column chromatography on silica gel eluting with cyclohexane/dichloromethane (80/20). The product was obtained as a maroonish oil and was stored at 4°C. (2.4 g, 35%). ^{1}H NMR (400.1 MHz, $CDCl_3$): δ = 3.27 (s, 4H, CH_2S), 1,34 (s, 18H, CH_3). RMN $^{13}C\{^1H\}$ (100.6 MHz, $CDCl_3$): δ = 79.5 (C≡C), 43.2 ($SC(CH_3)_3$),), 30.9 ($SC(CH_3)_3$), 17.2 ($C{\equiv}CCH_2S$). IR (ATR): 2959 (m), 2899 (m), 2862 (w), 1471 (w), 1459 (m), 1406 (w), 1391 (w), 1364 (s), 1237 (m), 1212 (w), 1160 (s), 933 (w), 848 (w), 812 (w), 740 (w), 706 (w) cm^{-1}.

CP synthesis

General procedure for the CP preparation

The reactions were performed in the dark under nitrogen atmosphere. Solutions of the organic ligand and the silver salt were prepared separately in 5 to 20 mL of a chosen solvent. After slow addition of the ligand solution to the silver salt one, the resulting reaction mixture was stirred for 2 hours at room temperature. Slow concentration of the solution in the dark yielded single crystals suitable for X-ray analysis. The crystals collected were washed with ethanol and dried under vacuum. To avoid degradation, they were stored in the dark in a freezer.

Synthesis of CP1

CP1 was obtained according to the general procedure by reaction of AgOTs (140 mg, 0.5 mmol) dissolved in 5 mL CH_3CN with L_{Ph} (203 mg, 0.75 mmol) dissolved in 5 mL CH_3CN. **CP1** was obtained as a white powder (215 mg, 63%). IR (ATR): 3061 (w), 2945 (w), 2918 (w), 1580 (w), 1479 (m), 1439 (m), 1339 (w), 1258 (w), 1220 (m), 1157 (s), 1116 (m), 1027 (m), 1004 (m), 816 (m), 737 (s), 674 (s), 561 (s), 477 (w) cm^{-1}. Anal. Calc for $C_{31}H_{28}AgO_3S_4$ (684.64): %C 54.38, %H 4.12, %S 18.73, found: %C 54.44, %H 4.05, %S 19.33.

Synthesis of CP2

CP2 was obtained according to the general procedure by reaction of AgOTs (279 mg, 1 mmol) dissolved in 5 mL MeOH with L_{Cy} (300 mg, 1.1 mmol) dissolved in 5 mL $CHCl_3$. **CP2** was obtained as a white powder (325 mg, 58%).IR (ATR): 2925 (m), 2854 (w), 1450 (w), 1416 (w), 1169 (m), 1121 (m), 1031 (m), 1006 (s), 885 (w), 819 (m), 677 (s), 563 (s) cm^{-1}. Anal. Calc for $C_{23}H_{33}AgO_3S_3$ (561.54): %C 49.37, %H 5.92, %S 17.13, found: %C 49.17, %H 5.91, %S 17.32.

Synthesis of CP3

CP3 was obtained according to the general procedure by reaction of AgOTs (279 mg, 1 mmol) dissolved in 10 mL CH_3CN with $L_{t\mathrm{Bu}}$ (253 mg, 1.1 mmol) dissolved in 5 mL CH_3CN. **CP3** was obtained as a white powder after slow evaporation of the solvent (398 mg, 75 %). IR (ATR): 2960 (w), 2922 (w), 1457 (w), 1403 (w), 1368 (w), 1261 (w), 1186 (s), 1163 (s), 1120 (s), 1031 (m), 1007 (s), 813 (m), 708 (w), 677 (s), 560 (s) cm^{-1}. Anal. Calc for $C_{19}H_{29}AgO_3S_3$ (509.47): %C 44.79, %H 5.74, %S 18.88, found: %C 44.55, %H 5.61, %S 18.49.

Synthesis of D1

A buffer layer of CH_2Cl_2 (1 mL) and CH_3CN (1 mL) were carefully layered over CH_2Cl_2 (2 mL) solution of $\mathbf{L_{Ph}}$ (135 mg, 0.5 mmol). Then, a solution of AgOTf (128 mg, 0.5 mmol) in CH_3CN (2 mL) was layered over the buffer layer. The solution was left closed in the dark for several weeks at room temperature, and white-yellow crystals were obtained (205 mg, 78%). IR (ATR): 3062 (w), 2978 (w), 1585 (w), 1474 (w), 1440 (m), 1414 (w), 1300 (s), 1229 (s), 1204 (s), 1180 (m), 1157 (s), 1070 (w), 1013 (s), 759 (s), 688 (s), 630 (s) cm^{-1}. Anal. Calc for $C_{17}H_{14}AgF_3O_3S_3$ (527.33): %C 38.72, %H 2.68, %S 18.24, found: %C 39.28, %H 2.92, %S 18.37.

Synthesis of CP4

A buffer layer of CH_2Cl_2 (1 mL) and CH_3CN (1 mL) were carefully layered over CH_2Cl_2 (2 mL) solution of $\mathbf{L_{Cy}}$ (140 mg, 0.5 mmol). Then, a solution of AgOTf (128 mg, 0.5 mmol) in CH_3CN (2 mL) was layered over the buffer layer. The solution was left closed in the dark for several weeks at room temperature, and a brown powder and some crystals were obtained (245 mg, 91%). IR (ATR) : 2919 (m), 2850 (w), 1440 (w), 1418 (w), 1339 (w), 1290 (m), 1229 (s), 1217 (s), 1157 (s), 1026 (s), 998 (m), 755 (w), 689 (w), 632 (s), 571 (m), 514 (m) cm^{-1}. Anal. Calc for $C_{17}H_{26}AgF_3O_3S_3$ (539.43 g/mol): %C 37.85; %H 4.86, %S 17.83, found: %C 35.96; %H 4.92, %S 17.99.

Synthesis of CP5

CP5 was obtained according to the general procedure by reaction of $AgCF_3CO_2$ (220 mg, 1 mmol) dissolved in 15 mL CH_3CN with L_{Cy} (280 mg, 1 mmol) dissolved in 2 mL CH_3CN. **CP5** was obtained as a light brown powder after slow evaporation of the solvent (405 mg, 81 %). IR (ATR): 2937 (m), 2858 (w), 1653 (s), 1447 (w), 1414 (w), 1401 (w), 1265 (w), 1238 (w), 1174 (s), 1132 (s), 998 (m), 887 (w), 827 (m), 795 (m), 719 (s), 695 (w) cm^{-1}. Anal. Calc for $C_{18}H_{26}AgF_3O_2S_2$ (503.38 g/mol): %C 42.95, %H 5.21, %S 12.74; found, %C 39.91; %H 4.96, %S 12.52.

Synthesis of CP6

CP6 was obtained according to the general procedure by reaction of $AgCF_3CO_2$ (440 mg, 2 mmol) dissolved in 15 mL CH_3CN with $L_{t\mathrm{Bu}}$ (230 mg, 1 mmol) dissolved in 2 mL CH_3CN. About 10 mL of ethanol were added and **CP6** was obtained as a slightly gray powder after slow evaporation of the solvent (350 mg, 62 %). IR (ATR): 2968 (m), 2927 (w), 2868 (w), 1667 (s), 1648 (s), 1461 (w), 1421 (m), 1399 (w), 1371 (m), 1158 (s), 1124 (s), 896 (w), 830 (m), 792 (m), 718 (s) cm^{-1}. Anal. Calc for $C_{30}H_{44}Ag_3F_9O_6S_4$ (1123.50 g/mol): %C 32.07, %H 3.95, %S 11.42, found: %C 31.78, %H 4.03, %S 10.43.

4- Antibacterial activity

Bacterial strains and growth conditions

Microbiological experiments were conducted with Gram-negative *Escherichia coli (E. coli* ATCC 25922) and Gram-positive *Staphylococcus aureus* (*S. aureus* ATCC 25923). Bacteria were stored at -80°C. Before the experiments, they were incubated overnight at 30°C on Lysogeny Broth (Miller-LB, 20 $g.L^{-1}$) agar (15g/L) plate for *E. coli* and at 37°C on Mueller-Hinton (MH, 25$g.L^{-1}$) agar (15g/L) plate for *S. aureus*. Then, a liquid pre-culture was prepared with one colony of *E. coli* or *S. aureus* in LB or MH media, respectively, and stirred overnight (90 rpm) at 30°C or 37°C, respectively. Bacterial concentration in liquid culture was estimated via UV-Vis spectroscopy (UV-2450 Shimadzu spectrophotometer) at 620 nm using a calibration curve. At this stage, the initial bacterial concentration is close to 10^9 $CFU.mL^{-1}$.

Minimal Inhibition Concentration (MIC) and Minimal Bactericidal Concentration (MBC) measurements

MICs values were determined by the two-fold dilution method. Experiments were performed in 96-well microplates as triplicate in culture media (LB for *E. coli* and MH for *S. aureus*), with an initial bacterial concentration of approximately 10^6 CFU.mL^{-1} in each well. The antibacterial compounds highest concentrations were prepared according to the following recipe: silver salts in distilled water, ligands in water/acetonitrile (94/6 % v/v) and CPs suspensions in culture media. These concentrations were then twofold serially diluted with broth. After overnight incubation at 30°C/37°C, MICs were determined as the lowest concentration of the compound with no visible bacterial growth. Sterility control (culture broth only), growth control (culture broth with bacteria) and death control (culture broth with bacteria and 50% ethanol) assessed the quality of each experiment.

MBCs determination was performed by measuring the optical density at 620 nm of the 96-well plate. MBCs values were taken when OD was less than 0.001×OD of the control growth.

Time-killing assays

Suspensions of *E. coli* in LB with initial concentration close to 10^9 CFU.mL^{-1} were centrifuged (5000×g, 5 min, 4°C). The supernatant was removed and replaced by the same quantity of PBS. This process was performed twice to remove any trace of media culture. The bacterial suspensions were diluted in PBS to obtain a concentration of 10^6 CFU.mL^{-1}. This bacterial suspension was incubated at 30°C with the CP at 1 µg Ag.mL^{-1}. Aliquots of 100 µL were withdrawn at different times, diluted 10, 100 and 1000 times in PBS, and spread onto LB + agar (20 g/L + 15 g/L) plates using Interscience EasySpiral automatic inoculator. After overnight incubation at 30°C, the CFUs were enumerated with a Interscience Colony Counter Scan 300. Controls were run without CP and experiments were performed in duplicate.

Cell culture

NHDFs from the abdomen were purchased from Promocell (reference C-12302). Cells were cultured in Dulbecco's modified Eagle's medium (DMEM) with 2% glutamine, complemented with 10% fetal bovine serum (FBS) and 1% penicillin-streptomycin (100 U/mL and 0.1 mg/mL, respectively), and incubated at 37 °C with 5% CO_2 in a humidified atmosphere. The cells were passaged every 3 or 4 days and seeded at 10 000 cells/cm^2 for culture maintenance.

Cytotoxicity Assays.

For the assessment of CPs'toxicity, 8×10^3 cell in DMEM without SVF were placed in each well of a 96-well plate (100 µL/well). Then for each CP, from an initial dilution in DMEM without SVF at 620 mg/mL Ag equivalent, a cascade dilution was carried out in DMEM without SVF to get the 8 working concentrations: 160 – 80 – 40 – 20 – 10 – 5 – 2.5 – 1.25 µg Ag /mL. 100 µL of each working suspension was added into three wells (triplicate). Controls were prepared by addition of cell media into the wells. The cells were incubated for 24 h at 37 °C and 5% CO_2 before microscopic observations and cytotoxicity assays.

The CP biocompatibility was evaluated using a LDH and a MTT assay. Cells in the positive control well were exposed to 0.75% v/v Triton X-100 for 30 min. Before the MTT assay, 10 μL of cell supernatants were collected and transferred to a new 96-well plate to assess cell necrosis by measuring LDH (lactate dehydrogenase) release. To this new plate were added 100 μL of LDH mix. After 30 min of incubation at room temperature, protected from light, 10 μL of the stop solution was then added. The absorbance was then read at 450 nm (Clariostar plate reader). After removal of the absorbance of the blank, the results are expressed in percent of the positive control (100% of necrotic cells with maximal LDH release). For the viability assay, in the first 96-well plate, we then removed 90 µL (remaining volume 100 µL) and added 10%v/v of MTT labeling agent (10 µL). The plate was then incubated for 4 hours at 37 °C and 5% CO2 for the viable cells to reduce the MTT into purple formazan salts. After this time, an equivalent volume (100 µL) of a HCl-propanol solution was added to dissolve the salts and the content of each well was gently stirred. The absorbance was then read at 570 nm. After removal of the absorbance of the blank, the results are expressed in percent of the negative control (100% viable cell with maximal mitochondrial activity).

5- X-ray Crystallography

X ray powder patterns were obtained at 295 K on a D8 Advance Bruker diffractometer using Ni-filtered K-α radiation. All crystal structures (**D1**, **CP1-CP6**) were determined using the *Bruker D8 Venture* four-circle diffractometer equipped with a *PHOTON II* CPAD detector by *Bruker AXS GmbH*. For all structural measurements, Mo *Kα* radiation was used. The APEX 4 Suite (v.2021.10-0)[57] software integrated with SAINT (integration) and SADABS (adsorption correction) programs by *Bruker AXS GmbH* were used for data collection. The processing and finalization of the crystal structure were performed using the Olex2 program.[58] The crystal structures were solved by the ShelXT[59] structure solution program using the *intrinsic phasing*

option, which were further refined by the ShelXL[60] refinement package using Least Squares minimization.[61] For the hydrogen atoms, the standard values of the SHELXL program were used with $U_{iso}(H) = -1.2\ U_{eq}(C)$ for CH_2 and CH and with $U_{iso}(H) = -1.5\ U_{eq}(C)$ for CH_3. Some H atoms were refined freely using independent values for each $U_{iso}(H)$. In compound **CP5** one CF3 group is positionally disordered and refined using free variables. The fluorine atoms F1, F2 and F3 were disordered with a ratio of 61.5:28.5. In compound **CP6** a CF_3COO and 2 CF_3 groups are positionally disordered and refined using free variables. The fluorine atom F3 was disordered with a ratio of 50:50, the atoms F5, F6 were disordered with a ratio of 55:45, the atoms F8, F9, C30 were disordered with a ratio of 55.4:44.6 and the oxygen atom O6 was disordered with a ratio of 54.4:45.6.

The crystallographic data for the structures of **CP1-CP6** and **D1** have been published as supplementary publication number 2364559 (**CP1**), 2364558 (**CP2**), 2364504 (**CP3**), 2364562 (**CP4),** 2364560 (**CP5**), 2364565 (**CP6**), 2364561 (**D1**) in the Cambridge Crystallographic Data Centre. A copy of these data can be obtained for free by applying to CCDC, 12 Union Road, Cambridge CB2 IEZ, UK, fax: 144-(0)1223-336033 or e-mail: deposit@ccdc.cam.ac.uk.

Associated content

Supporting Information. Crystallographic data in CIF file, summary of X-ray data collection and refinement for all structures studied, structure views of **CP1-CP6** and **D1** with hydrogen bondings, Powder X-Ray Patterns of **CP1-CP6** and **D1**, TGA traces of **CP1-CP6** and **D1**, fibroblasts viability of **CP1-CP6** and **D1**. The following files are available free of charge on the ACS publication website at http://pubs.acs.org.

Author information

* E-mail: lydie.viau@univ-fcomte.fr; isabelle.jourdain@univ-fcomte.fr

Acknowledgements

Q.G. thanks the Ministère de l'Enseignement Supérieur et de la Recherche for his PhD scholarship. This work has been achieved in the frame of the EIPHI Graduate school (contract

"ANR-17-EURE-0002"). The authors thank Marie-Laure Léonard from ESIREM Dijon, France for obtaining the TGA results and Dr. Nicolas Rouge from the Plateforme Chimie UTINAM for recording the SEM images. C. Strohmann, and *J.-L. Kirchhoff* thank the Deutsche Forschungsgemeinschaft *DFG*, the Fonds der Chemischen Industrie and the Konrad-Adenauer-Stiftung for financial support. We are indebted to S. Adache from SynBioN (Université de Lorraine-CNRS – http://synbion.univ-lorraine.fr/accueil/) for the elemental analyses.

Author Contributions

This manuscript was written through the contributions of all authors. All authors have given approval to the final version of the manuscript.

References

1. Fleming, A., On the antibacterial action of cultures of a penicillium, with special reference to their use in the isolation of B. influenzae. *Brit. J. Exp. Pathol* **1929,** *10* (3), 226.
2. Abraham, E.; Chain, E., An enzyme from bacteria able to destroy penicillin. 1940. *Rev. Infect. Dis.* **1988,** *10* (4), 677-678.
3. Bérdy, J., Thoughts and facts about antibiotics: Where we are now and where we are heading. *J. Antibiot.* **2012,** *65* (8), 385-395.
4. Alexander, J. W., History of the medical use of silver. *Surg Infect* **2009,** *10* (3), 289-92.
5. Barillo, D. J.; Marx, D. E., Silver in medicine: A brief history BC 335 to present. *Burns* **2014,** *40*, S3-S8.
6. Pelgrift, R. Y.; Friedman, A. J., Nanotechnology as a therapeutic tool to combat microbial resistance. *Adv. Drug Deliver. Rev.* **2013,** *65* (13), 1803-1815.
7. Klasen, H. J., Historical review of the use of silver in the treatment of burns. I. Early uses. *Burns* **2000,** *26* (2), 117-130.
8. Fox, C. L.; Modak, S. M., Mechanism of Silver Sulfadiazine Action on Burn Wound Infections. *Antimicrob. Agents Chemother.* **1974,** *5* (6), 582-588.
9. Chernousova, S.; Epple, M., Silver as Antibacterial Agent: Ion, Nanoparticle, and Metal. *Angew. Chem. Int. Ed.* **2013,** *52* (6), 1636-1653.

10. Abram, S.-L.; Fromm, K. M., Handling (Nano)Silver as Antimicrobial Agent: Therapeutic Window, Dissolution Dynamics, Detection Methods and Molecular Interactions. *Chem. Eur. J.* **2020,** *26* (48), 10948-10971.

11. Hamad, A.; Khashan, K. S.; Hadi, A., Silver Nanoparticles and Silver Ions as Potential Antibacterial Agents. *J. Inorg. Organomet. Polym.* **2020,** *30* (12), 4811-4828.

12. Zheng, K.; Setyawati, M. I.; Leong, D. T.; Xie, J., Antimicrobial silver nanomaterials. *Coord. Chem. Rev.* **2018,** *357*, 1-17.

13. Bruna, T.; Maldonado-Bravo, F.; Jara, P.; Caro, N., Silver Nanoparticles and Their Antibacterial Applications. *Int. J. Mol. Sci.* **2021,** *22* (13), 7202.

14. Jo, Y.; Garcia, C. V.; Ko, S.; Lee, W.; Shin, G. H.; Choi, J. C.; Park, S.-J.; Kim, J. T., Characterization and antibacterial properties of nanosilver-applied polyethylene and polypropylene composite films for food packaging applications. *Food Bioscience* **2018,** *23*, 83-90.

15. Azlin-Hasim, S.; Cruz-Romero, M. C.; Morris, M. A.; Cummins, E.; Kerry, J. P., Effects of a combination of antimicrobial silver low density polyethylene nanocomposite films and modified atmosphere packaging on the shelf life of chicken breast fillets. *Food Packag. Shelf Life* **2015,** *4*, 26-35.

16. Sargin, I., Chapter 14 - Polymer–silver composites for food packaging. In *Nanostructured Materials for Food Packaging Applications*, Jacob, J.; Cacciotti, I.; Thomas, S., Eds. Elsevier: 2024; pp 323-344.

17. Trotta, F.; Da Silva, S.; Massironi, A.; Mirpoor, S. F.; Lignou, S.; Ghawi, S. K.; Charalampopoulos, D., Silver Bionanocomposites as Active Food Packaging: Recent Advances & Future Trends Tackling the Food Waste Crisis. *Polymers* **2023,** *15* (21), 4243.

18. Corrêa, J. M.; Mori, M.; Sanches, H. L.; Cruz, A. D. d.; Poiate Jr., E.; Poiate, I. A. V. P., Silver Nanoparticles in Dental Biomaterials. *Int. J. Biomater.* **2015,** *2015* (1), 485275.

19. Venkataraman, D.; Du, Y.; Wilson, S. R.; Hirsch, K. A.; Zhang, P.; Moore, J. S., A Coordination Geometry Table of the d-Block Elements and Their Ions. *J. Chem. Educ.* **1997,** *74* (8), 915.

20. Medici, S.; Peana, M.; Crisponi, G.; Nurchi, V. M.; Lachowicz, J. I.; Remelli, M.; Zoroddu, M. A., Silver coordination compounds: A new horizon in medicine. *Coord. Chem. Rev.* **2016,** *327-328*, 349-359.

21. Jaros, S. W.; Florek, M.; Bażanów, B.; Panek, J.; Krogul-Sobczak, A.; Oliveira, M. C.; Król, J.; Śliwińska-Hill, U.; Nesterov, D. S.; Kirillov, A. M.; Smoleński, P., Silver

Coordination Polymers Driven by Adamantoid Blocks for Advanced Antiviral and Antibacterial Biomaterials. *ACS Appl. Mater. Interfaces* **2024,** *16* (11), 13411-13421.

22. Jaros, S. W.; Guedes da Silva, M. F. C.; Król, J.; Conceição Oliveira, M.; Smoleński, P.; Pombeiro, A. J. L.; Kirillov, A. M., Bioactive Silver–Organic Networks Assembled from 1,3,5-Triaza-7-phosphaadamantane and Flexible Cyclohexanecarboxylate Blocks. *Inorg. Chem.* **2016,** *55* (4), 1486-1496.

23. Jaros, S. W.; Guedes da Silva, M. F. C.; Florek, M.; Oliveira, M. C.; Smoleński, P.; Pombeiro, A. J. L.; Kirillov, A. M., Aliphatic Dicarboxylate Directed Assembly of Silver(I) 1,3,5-Triaza-7-phosphaadamantane Coordination Networks: Topological Versatility and Antimicrobial Activity. *Cryst. Growth Des.* **2014,** *14* (11), 5408-5417.

24. Lu, X.; Ye, J.; Zhang, D.; Xie, R.; Bogale, R. F.; Sun, Y.; Zhao, L.; Zhao, Q.; Ning, G., Silver carboxylate metal–organic frameworks with highly antibacterial activity and biocompatibility. *J. Inorg. Biochem.* **2014,** *138*, 114-121.

25. Xie, B.-P.; Chai, J.-W.; Fan, C.; Ouyang, J.-H.; Duan, W.-J.; Sun, B.; Chen, J.; Yuan, L.-X.; Xu, X.-Q.; Chen, J.-X., Water-Stable Silver-Based Metal–Organic Frameworks of Quaternized Carboxylates and Their Antimicrobial Activity. *ACS Appl. Bio Mater.* **2020,** *3* (12), 8525-8531.

26. Nong, W.; Wu, J.; Ghiladi, R. A.; Guan, Y., The structural appeal of metal–organic frameworks in antimicrobial applications. *Coord. Chem. Rev.* **2021,** *442*, 214007.

27. Seyedpour, S. F.; Arabi Shamsabadi, A.; Khoshhal Salestan, S.; Dadashi Firouzjaei, M.; Sharifian Gh, M.; Rahimpour, A.; Akbari Afkhami, F.; Shirzad Kebria, M. R.; Elliott, M. A.; Tiraferri, A.; Sangermano, M.; Esfahani, M. R.; Soroush, M., Tailoring the Biocidal Activity of Novel Silver-Based Metal Azolate Frameworks. *ACS Sustain. Chem. Eng.* **2020,** *8* (20), 7588-7599.

28. Cardoso, J. M. S.; Galvão, A. M.; Guerreiro, S. I.; Leitão, J. H.; Suarez, A. C.; Carvalho, M. F. N. N., Antibacterial activity of silver camphorimine coordination polymers. *Dalton Trans.* **2016,** *45* (16), 7114-7123.

29. Kulovi, S.; Pradhan, A.; Maiti , S.; Puschmann, H.; Zangrando, E.; Dalai, S., Polymorphism in [Ag(bpetan)]n Coordination Polymers with Nitrate and Isophthalate Anions: Photocatalytic and Antibacterial Activity, Hemolysis Assay and Study of Cytotoxicity. *ChemistrySelect* **2020,** *5* (11), 3337-3346.

30. Chevrier, I.; Sagué, J. L.; Brunetto, P. S.; Khanna, N.; Rajacic, Z.; Fromm, K. M., Rings, chains and helices: new antimicrobial silver coordination compounds with (iso-)nicotinic acid derivatives. *Dalton Trans.* **2013,** *42* (1), 217-231.

31. Fromm, K. M., Silver coordination compounds with antimicrobial properties. *Appl. Organomet. Chem.* **2013,** *27* (12), 683-687.

32. Soleymani-Babadi, S.; Beheshti, A.; Bahrani-Pour, M.; Mayer, P.; Motamedi, H.; Trzybiński, D.; Wozniak, K., Synthesis, Structural Characterization, Photophysical Properties, and Antibacterial Assessment of Silver(I)-Thione Coordination Polymers Based on a Competition between Nitrate Anion and Coanions CF3SO3–, ClO4–, BF4–, PF6–, and SbF6–. *Cryst. Growth Des.* **2019,** *19* (9), 4934-4948.

33. Pearson, R. G.; Songstad, J., Application of the Principle of Hard and Soft Acids and Bases to Organic Chemistry. *J. Am. Chem. Soc.* **1967,** *89* (8), 1827-1836.

34. Gaudillat, Q.; Krupp, A.; Zwingelstein, T.; Humblot, V.; Strohmann, C.; Jourdain, I.; Knorr, M.; Viau, L., Silver-based coordination polymers assembled by dithioether ligands: potential antibacterial materials despite received ideas. *Dalton Trans.* **2023,** *52* (18), 5859-5864.

35. Knorr, M.; Viau, L.; Knauer, L.; Strohmann, C.; Rousselin, Y.; Kubicki, M. M., Polymeric CuX coordination compounds assembled from acetylenic thioether ligands $RSCH_2C{\equiv}CCH_2R$ (R = C_6H_{11}, t-Bu): effect of the RS-group, halide and stoichiometry on the network architecture and the luminescence properties. *CrystEngComm* **2024,** *26* (22), 2953-2975.

36. Yang, L.; Powell, D. R.; Houser, R. P., Structural variation in copper(i) complexes with pyridylmethylamide ligands: structural analysis with a new four-coordinate geometry index, τ4. *Dalton Trans.* **2007,** (9), 955-964.

37. Bondi, A., van der Waals Volumes and Radii. *J. Phys. Chem.* **1964,** *68* (3), 441-451.

38. Schmidbaur, H.; Schier, A., Argentophilic Interactions. *Angew. Chem. Int. Ed.* **2015,** *54* (3), 746-784.

39. Awaleh, M. O.; Badia, A.; Brisse, F., Coordination Networks with Flexible Ligands Based on Silver(I) Salts: Complexes of 1,3-Bis(phenylthio)propane with Silver(I) Salts of PF_6^-, CF_3COO^-, $CF_3CF_2COO^-$, $CF_3CF_2CF_2COO^-$, p-TsO^-, and CF_3SO_3. *Inorg. Chem.* **2005,** *44* (22), 7833-7845.

40. Cui, L.-N.; Li, Z.-F.; Jin, Q.-H.; Xin, X.-L.; Zhang, C.-L., "Honeycomb" (6, 3) network constructed from 14-membered ring [Ag2(μ-dppb)2]: Synthesis, characterization and crystal structures of two silver(I) complexes of bis(diphenylphosphino)butane. *Inorg. Chem. Commun.* **2012,** *20*, 126-130.

41. Addison, A. W.; Rao, T. N.; Reedijk, J.; van Rijn, J.; Verschoor, G. C., Synthesis, structure, and spectroscopic properties of copper(II) compounds containing nitrogen–sulphur

donor ligands; the crystal and molecular structure of aqua[1,7-bis(N-methylbenzimidazol-2′-yl)-2,6-dithiaheptane]copper(II) perchlorate. *J. Chem. Soc., Dalton Trans.* **1984,** (7), 1349-1356.

42. Awaleh, M. O.; Badia, A.; Brisse, F.; Bu, X.-H., Synthesis and Characterization of Silver(I) Coordination Networks Bearing Flexible Thioethers: Anion versus Ligand Dominated Structures. *Inorg. Chem.* **2006,** *45* (4), 1560-1574.

43. Vujasinović, I.; Veljković, J.; Molčanov, K. i.; Kojić-Prodić, B.; Mlinarić-Majerski, K., Thiamacrocyclic Lactones: New Ag(I)-Ionophores. *J. Org. Chem.* **2008,** *73* (23), 9221-9227.

44. Helttunen, K.; Nissinen, M., Inverted molecular cups: 1-D and 2-D Ag(i) coordination polymers from resorcinarene bis-thiacrowns. *CrystEngComm* **2016,** *18* (26), 4944-4951.

45. Ristova, M.; Pejov, L.; Žugić, M.; Šoptrajanov, B., Experimental IR, Raman and ab initio molecular orbital study of the 4-methylbenzenesulfonate anion. *J. Mol. Struct.* **1999,** *482-483*, 647-651.

46. Johnston, D. H.; Shriver, D. F., Vibrational study of the trifluoromethanesulfonate anion: unambiguous assignment of the asymmetric stretching modes. *Inorg. Chem.* **1993,** *32* (6), 1045-1047.

47. Szłyk, E.; Szymańska, I.; Surdykowski, A.; Głowiak, T.; Wojtczak, A.; Goliński, A., X-Ray crystal structure of $[Ag_4(\mu\text{-dppm})_2(\mu\text{-}C_2F_5COO)_4]$. Synthesis and spectroscopy of silver(i) perfluorinated carboxylate complexes with bis(diphenylphosphino)methane. *Dalton Trans.* **2003,** (17), 3404-3410.

48. Reger, D. L.; Semeniuc, R. F.; Silaghi-Dumitrescu, I.; Smith, M. D., Influences of Changes in Multitopic Tris(pyrazolyl)methane Ligand Topology on Silver(I) Supramolecular Structures. *Inorg. Chem.* **2003,** *42* (12), 3751-3764.

49. Wing-Wah Yam, V.; Kam-Wing Lo, K., Luminescent polynuclear d10 metal complexes. *Chem. Soc. Rev.* **1999,** *28* (5), 323-334.

50. Shi, J.; Song, F.; Ge, H.; Gao, Y.; Guo, S., Synthesis, characterization and antimicrobial property in vitro of supramolecular coordination polymers bearing brominated Schiff base ligand. *J. Inorg. Biochem.* **2022,** *236*, 111939.

51. Wang, K.; Ma, X.; Shao, D.; Geng, Z.; Zhang, Z.; Wang, Z., Coordination-Induced Assembly of Coordination Polymer Submicrospheres: Promising Antibacterial and in Vitro Anticancer Activities. *Cryst. Growth Des.* **2012,** *12* (7), 3786-3791.

52. Pettinari, C.; Pettinari, R.; Di Nicola, C.; Tombesi, A.; Scuri, S.; Marchetti, F., Antimicrobial MOFs. *Coord. Chem. Rev.* **2021,** *446*, 214121.

53. Lu, X.; Ye, J.; Sun, Y.; Bogale, R. F.; Zhao, L.; Tian, P.; Ning, G., Ligand effects on the structural dimensionality and antibacterial activities of silver-based coordination polymers. *Dalton Trans.* **2014,** *43* (26), 10104-10113.

54. Jo, J. H.; Kim, H.-C.; Huh, S.; Kim, Y.; Lee, D. N., Antibacterial activities of Cu-MOFs containing glutarates and bipyridyl ligands. *Dalton Trans.* **2019,** *48* (23), 8084-8093.

55. Hamilton-Miller, J. M. T.; Shah, S.; Smith, C., Silver Sulphadiazine: A Comprehensive in vitro Reassessment. *Chemotherapy* **1993,** *39* (6), 405-409.

56. Zwingelstein, T.; Figarol, A.; Luzet, V.; Crenna, M.; Bulliard, X.; Finelli, A.; Gay, J.; Lefèvre, X.; Pugin, R.; Laithier, J.-F.; Chérioux, F.; Humblot, V., A Kinetic Approach to Synergize Bactericidal Efficacy and Biocompatibility in Silver-Based Sol–Gel Coatings. *ACS Omega* **2024,** *9* (23), 24574-24583.

57. Bruker. *Apex 4*; Bruker AXS Inc.: Madison, WI, USA, 2021.

58. Dolomanov, O. V.; Bourhis, L. J.; Gildea, R. J.; Howard, J. A. K.; Puschmann, H., OLEX2: a complete structure solution, refinement and analysis program. *J. Appl. Crystallogr.* **2009,** *42* (2), 339-341.

59. Sheldrick, G., SHELXT - Integrated space-group and crystal-structure determination. *Acta Cryst . A* **2015,** *71* (1), 3-8.

60. Sheldrick, G., Crystal structure refinement with SHELXL. *Acta Cryst. C* **2015,** *71* (1), 3-8.

61. Sheldrick, G., A short history of SHELX. *Acta Cryst . A* **2008,** *64* (1), 112-122.

Synopsis

Six molecular complexes and coordination polymers have been prepared by coordination of soft donor acetylenic dithioether ligands on various soft Lewis Acid Ag(I) salts and their antibacterial properties were determined against both gram-positive and gram-negative bacteria. In addition to their antibacterial properties three of them are non-cytotoxic.

Table of content graphic